

Monocrystalline Si/ β -Ga₂O₃ p-n heterojunction diodes fabricated via grafting

Jiarui Gong^{1,a)}, Donghyeok Kim^{1,a)}, Hokyung Jang^{1,a)}, Fikadu Alema^{2,a)}, Qingxiao Wang^{3,a)}, Tien Khee Ng³, Shuoyang Qiu¹, Jie Zhou¹, Xin Su¹, Qinchen Lin¹, Ranveer Singh¹, Haris Abbasi¹, Kelson Chabak⁴, Gregg Jessen⁴, Clincy Cheung⁵, Vincent Gambin⁵, Shubhra S. Pasayat¹, Andrei Osinsky^{2, b)}, Boon, S. Ooi^{3, b)}, Chirag Gupta^{1,b)}, Zhenqiang Ma^{1,b)}

¹*Department of Electrical and Computer Engineering, University of Wisconsin-Madison, Madison, Wisconsin, 53706, USA*

²*Agnitron Technology Incorporated, Chanhassen, MN 55317, USA*

³*Department of Electrical and Computer Engineering, King Abdullah University of Science and Technology, Thuwal 23955-6900, Saudi Arabia*

⁴*Air Force Research Laboratory, Dayton, OH 45433, USA*

⁵*Northrop Grumman, Redondo Beach, CA 90278, USA*

a) These authors contributed equally to this work.

b) Author to whom correspondence should be addressed. Electronic mail: mazq@engr.wisc.edu, cgupta9@wisc.edu, andrei.osinsky@agnitron.com, boon.ooi@kaust.edu.sa

Abstract

The β -Ga₂O₃ has exceptional electronic properties with vast potential in power and RF electronics. Despite the excellent demonstrations of high-performance unipolar devices, the lack of p-type doping in β -Ga₂O₃ has hindered the development of Ga₂O₃-based bipolar devices. The approach of p-n diodes formed by polycrystalline p-type oxides with n-type β -Ga₂O₃ can face severe challenges in further advancing the β -Ga₂O₃ bipolar devices due to their unfavorable band alignment and the poor p-type oxide crystal quality. In this work, we applied the semiconductor grafting approach to fabricate monocrystalline Si/ β -Ga₂O₃ p-n diodes for the first time. With enhanced concentration of oxygen atoms at the interface of Si/ β -Ga₂O₃, double side surface passivation was achieved for both Si and β -Ga₂O₃ with an interface D_{it} value of $1-3 \times 10^{12} / \text{cm}^2 \cdot \text{eV}$. A Si/ β -Ga₂O₃ p-n diode array with high fabrication yield was demonstrated along with a diode rectification of 1.3×10^7 at ± 2 V, a diode ideality factor of 1.13 and avalanche reverse breakdown characteristics. The diodes C-V shows frequency dispersion-free characteristics from 10 kHz to 2 MHz. Our work has set the foundation toward future development of β -Ga₂O₃-based transistors.

1. Introduction

Beta-phase gallium oxide (β -Ga₂O₃), an ultrawide-bandgap semiconductor, has attracted substantial attention in recent years due to its exceptional electronic properties and its vast potential in power electronics, solar-blind optoelectronics, and even potentially in radio-frequency electronics [1, 2]. With an ultrawide bandgap of 4.9 eV [3], a high breakdown electrical field of 10.3 MV/cm [2], a high electron saturation velocity (1.1×10^7 cm/s) [2], excellent thermal stability, and mature growth techniques [1], β -Ga₂O₃ is expected to generate impact in high-voltage, high-power, and high-temperature application. Various epitaxy techniques, including metalorganic chemical vapor deposition (MOCVD) [4-6], molecular-beam epitaxy [7, 8], and halide vapor phase epitaxy [9, 10], have been successfully demonstrated to produce high-quality epitaxial layers for device development. Furthermore, the easy availability of the native bulk substrates with a large diameter promises a lower cost through mass production in the industry in the future.

Despite these attractive properties of β -Ga₂O₃ and the excellent unipolar devices demonstrated, e.g., Schottky diodes [11-13] and field-effect transistors [14-17], there are some critical challenges to be addressed. For instance, the long-standing issue of lack of p-type doping in β -Ga₂O₃ has persisted. The p-type doping inefficiency stems from high ionization energy of acceptors [18, 19] when using the common dopants in Ga₂O₃. In the meantime, low hole mobility of merely around 41.4 cm²/V·s in β -Ga₂O₃ [18] further hinders its potential application in high-speed electronics. As a result, the design and fabrication of high-performance bipolar Ga₂O₃ devices, such as p-n diodes, which are the building blocks of more complicated bipolar devices like bipolar transistors, are of vital importance in advancing the β -Ga₂O₃ related device technologies, however, the progress along this direction is still in the research and development stage.

There were some attempts in developing β -Ga₂O₃-based p-n diodes. Depositing p-type oxides on n-type β -Ga₂O₃ showed p-n diodes with good rectification ratios [20-23]. However, the deposited p-type oxides are polycrystalline and the low crystal quality of these oxides limit the p-n diodes performance and would be infeasible for next-step triodes (e.g., transistors) device applications. To develop high-performance β -Ga₂O₃ based p-n diodes and other more complicated triode devices, monocrystalline p-type semiconductors like Si, GaAs, InP etc. are highly preferred.

In general, direct materials/wafer bonding/fusion of two monocrystalline semiconductors often leads to an interface layer having a high density of traps [24-43]. These traps serving as recombination and generation centers cause non-ideal rectification current-voltage (I-V) behavior in p-n junctions, including high ideality factors, high reverse-bias leakage current, difficulty to achieve avalanche breakdown and impossible to reach desired depletion width. As for β -Ga₂O₃, the wafer bonding of p-type diamond with n-type β -Ga₂O₃ showed limited device performance due to both high density of interfacial defects and unfavorable band alignment [44]. To overcome the issues associated with direct bonding/fusion, the semiconductor grafting approach [45] was introduced. The key feature of the grafting approach is that an ultrathin interfacial layer (e.g., ultrathin oxide etc.) is inserted between two grafted semiconductors with arbitrary lattice structures (and lattice constants), which forms chemical bonding with both semiconductors and physically separate them. The major physical functions of the interfacial layer are double side passivation and effective quantum tunneling. The double-side passivation function passivates the dangling bonds of the semiconductors surfaces thereby reducing the surface density of states, and with the minimum recombination from the passivation, both electrons and holes can transport across the interface with negligible loss via quantum tunneling. Consequently, the resultant grafted junctions can function like lattice-matched ones formed by epitaxy.

In the following paragraphs, the design of grafted Si/ β -Ga₂O₃ p-n junctions is described. First, the double-side passivation requirement in grafting is considered. As mentioned earlier, generally, an ultrathin oxide is inserted between two monocrystalline semiconductors to realize double-side passivation. In the case of β -Ga₂O₃, the interface ultrathin oxide can be Al₂O₃ or other types of oxides. However, the evidence of having almost no Fermi level pinning in previously demonstrated Schottky diodes [46, 47] strongly signifies that the surface of β -Ga₂O₃ is self-passivated. As a result, inserting a foreign ultrathin oxide like the Al₂O₃ to passivate the surface of β -Ga₂O₃ as practiced earlier [45] can be omitted in this case. By eliminating the extra foreign oxide, a thinner interface can be achieved to facilitate charge carrier transport across it. Moreover, according to the known band alignment between Si and Ga₂O₃, Ga₂O₃ can also passivate Si surface [2]. Therefore, the surface GaO_x layer itself on top of the β -Ga₂O₃ is expected, to some extent, to fulfill the double-side passivation requirement, as needed for successful grafting between Si and β -Ga₂O₃. To enhance the double-side passivation of the GaO_x layer, it is natural to further enrich the oxygen atoms of the surface of the β -Ga₂O₃, considering that it is the oxygen atoms that render the passivation functions.

Second, the design of interface for effective quantum tunneling is considered. When forming Si/ β -Ga₂O₃ heterointerface the surface oxygen atoms of the β -Ga₂O₃ layer will react with the surface Si atoms to passivate the Si surface dangling bonds via a thermal process, which may lead to the possible formation of a SiGaO_x layer at the interface. To make the interface SiGaO_x layer meet the requirement of effective quantum tunneling for charge carriers transporting across the interface, the interfacial SiGaO_x layer should be maintained as thin as possible. This requirement imposes a low thermal budget to be applied to the heterojunction grafting process in order to avoid an excessive atomic interdiffusion between the two semiconductors, which otherwise can lead to a thick interface layer. On the other hand, the planned thermal budget must be sufficient such that a strong chemical bonding can form between the Si and the β -

Ga₂O₃, enabling mechanical robustness of the finally grafted heterostructures. It is noted that the above Si/ β -Ga₂O₃ interface design considerations to satisfy the requirements of both sufficient double-side passivation and effective quantum tunneling differ much from that of materials bonding with surface activation (*i.e.*, surface activated bonding (SAB)) [48].

Our experiments were performed accordingly. First, a β -Ga₂O₃ epi substrate was grown. Then the surface of the β -Ga₂O₃ substrate was oxygen-enriched. We used X-ray photoelectron spectroscopy (XPS) analysis to verify the surface oxygen enrichment condition and study the surface atomic bonding conditions of the β -Ga₂O₃. A monocrystalline Si membrane was fabricated and transferred to the β -Ga₂O₃ substrate to form Si/ β -Ga₂O₃ heterojunctions, followed by the Si/ β -Ga₂O₃ p-n diode array fabrication. Scanning tunneling electron microscopy (STEM) analysis was carried out to examine the grafted Si/ β -Ga₂O₃ interface. The p-n diodes were also characterized via I-V and capacitance-voltage (C-V) analysis to understand the interface density of states (D_{it}) of the grafted heterostructures.

2. Results and Discussion

Figure 1 shows the detailed information of the β -Ga₂O₃ epi substrate. Figure 1(a) shows an optical image of a piece of diced β -Ga₂O₃ epi substrate ($15 \times 10 \text{ mm}^2$) with its crystal angle illustrated. The full-width of the half maximum (FWHM) of the XRD 2 theta-omega scan of β -Ga₂O₃ (020) peak is 144" (Figure 1(b)). The root-mean-square surface roughness (R_q) measured by AFM in a scanning area of $2 \times 2 \text{ }\mu\text{m}^2$ is 0.76 nm (Figure 1(c)). The smoothness of the surface of the β -Ga₂O₃ facilitates the grafting process with Si.

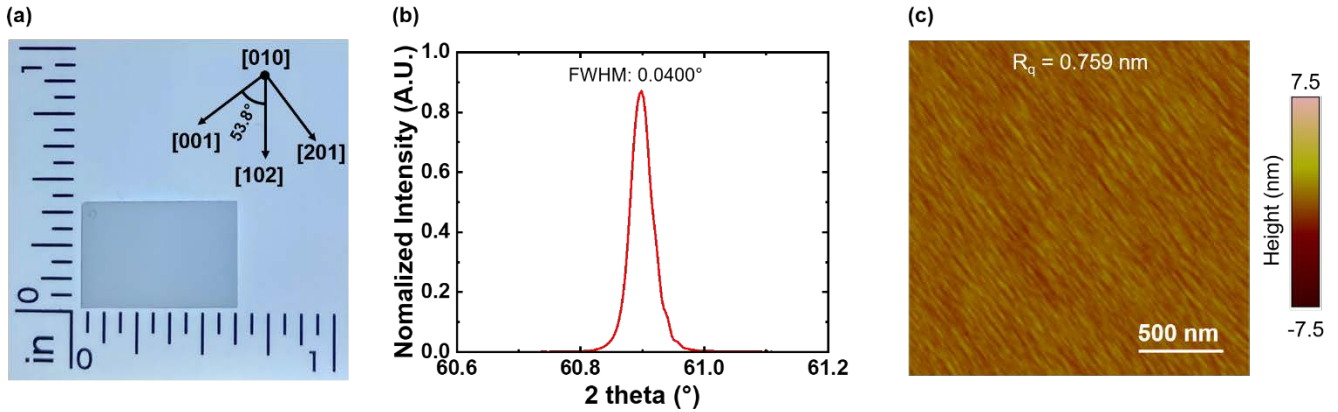


Figure 1. (a) An optical image of the β -Ga₂O₃ epi sample. (b) The 2 theta-omega XRD spectrum of the (002) peak from the as-grown β -Ga₂O₃ epi sample. (c). An AFM image taken on the epi surface ($2 \times 2 \mu\text{m}^2$) of the β -Ga₂O₃ sample. The R_q value is 0.76 nm.

Figure 2(a) shows an optical image of a patterned p+ SOI sample with hole arrays dry-etched through the top Si layer. The center square area to be released as membrane is $2.6 \times 2.6 \text{mm}^2$. The hole size is $9 \times 9 \mu\text{m}^2$, as shown in the zoomed-in optical microscopic image. The blue area is BOX, which is exposed by RIE etching. The outer frame Si area (with of $3.8 \text{mm} \times 3.8 \text{mm}$) without holes serve as a square anchor, which is not released by HF, with three Si ribbons ($300 \mu\text{m} \times 300 \mu\text{m}$) connecting each of the four sides of the square anchor to the center Si membrane. Figure 2(b) shows an image of the p+ Si membrane released inside the HF solution. The undercut process by HF solution can remove the BOX layer underneath the Si membrane area and the ribbons. Figure 2(c) shows the p+ Si membrane sitting on its original Si handling substrate after the HF release process was completed. Figure 2(d) shows an optical image of the picked Si membrane sitting on a PDMS stamp. The view of the surface is from the backside (which was in contact with the BOX layer before the undercut process) of the membrane. Figure 2(e) shows an AFM image of the backside of the Si NM sitting on the PDMS stamp with an R_q of 0.15 nm. Figure 2(f) shows the XRD 2 theta-omega spectrum of a Si membrane transferred to a β -Ga₂O₃ substrate,

from which the monocrystalline features of both Si and β -Ga₂O₃ can be clearly observed. The Raman spectra of both the Si/ β -Ga₂O₃ stack and the standalone β -Ga₂O₃ substrate are shown in Figure 2(g). The Si peak was observed at 517.2 cm⁻¹.

Bulk Si [49] and β -Ga₂O₃ [50] have a large difference of thermal expansion coefficients. As the Si thickness is reduced, it can accommodate more mechanical strain [51] than a bulk substrate. In addition, Si membrane is very flexible and much more compliant than its rigid counterpart and can be fabricated into any sizes, ranging from tens of microns to inches, for transfer printing. As a result, monocrystalline Si membrane is considered more advantageous than bulk Si when forming heterojunctions between Si and β -Ga₂O₃.

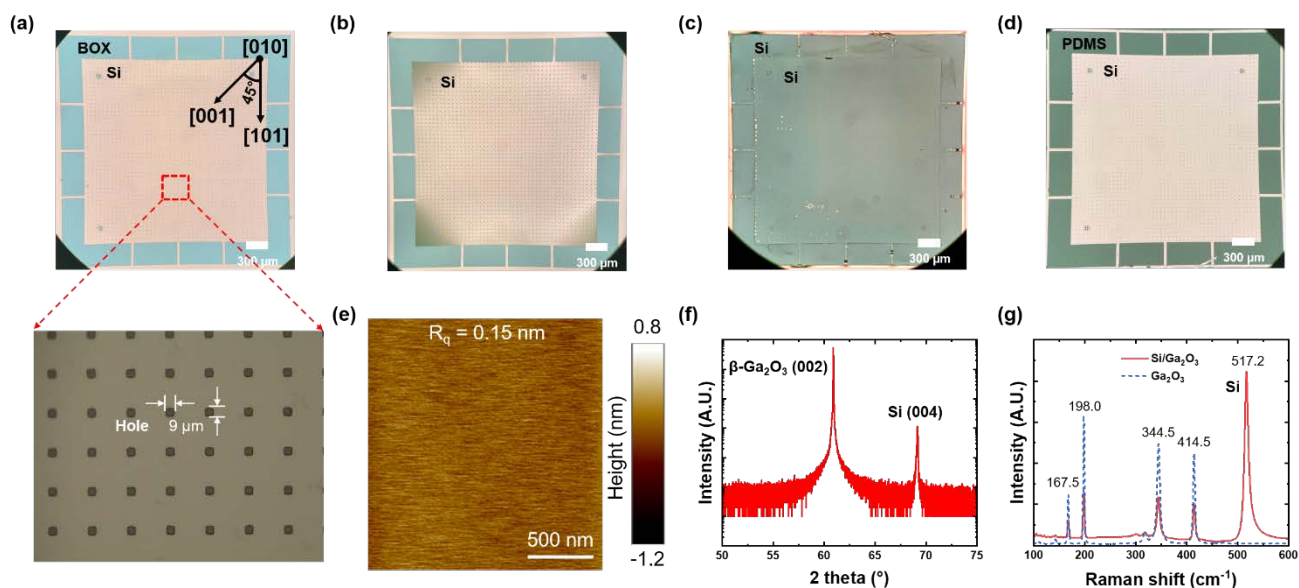


Figure 2. (a)-(d) Optical microscopic images of p+ Si membrane fabrication. (a) An image of a patterned p+ SOI substrate with hole arrays formed by RIE along with a magnified view to show the etched holes. (b) An image of the patterned SOI being released inside HF solution. The center Si membrane was floating in the HF solution while being anchored by the edge frame. (c) An image of the p+ Si membrane sitting on its handling Si substrate right after the release process was completed. The p+ Si membrane remains

flat. (d) An image of the p+ Si membrane attached to a PDMS stamp after being picked up. (e) The AFM image of the backside of the p+ Si membrane with a R_q value of 0.15 nm. (f) XRD spectrum of a p+ Si membrane transferred to a β -Ga₂O₃ substrate. (g) Raman spectra of the Si/ β -Ga₂O₃ stack (red solid) and the standalone β -Ga₂O₃ substrate (blue dash).

Figure 3(a) shows an optical microscopic image of the fabricated Si/ β -Ga₂O₃ p-n diode array along with the schematic illustration of the vertical layer structures (Figure 3(b)). The fabricated diode array was cleaved into two halves along the (001) plane. The entire array consists of 336 diodes, all having the same anode metal size, and the fabrication yield is close to 100%. No visible Si membrane or anode metal peeling off was observed. A detailed view of one individual diode is shown in Figure 3(c).

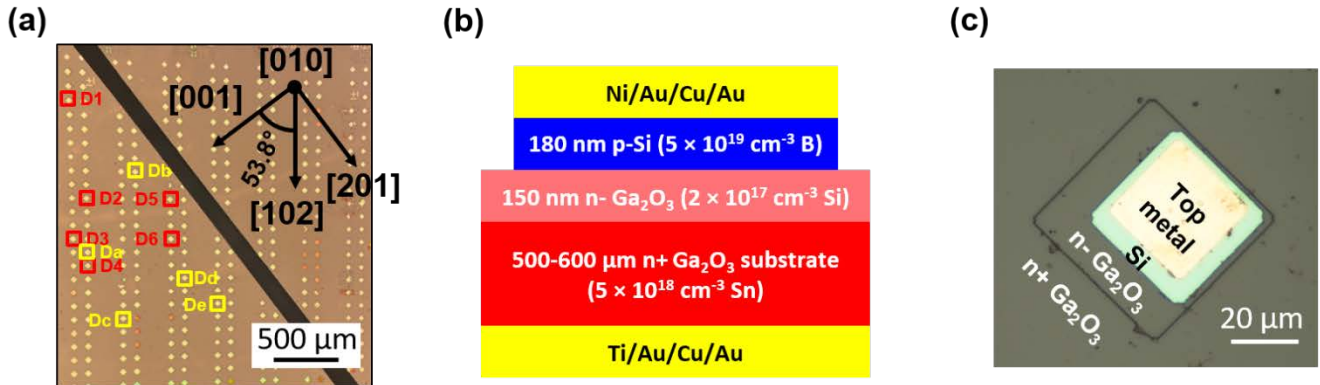


Figure 3. (a) An optical microscopic image of the fabricated Si/ β -Ga₂O₃ p-n diode array consisting of 336 diodes. The labeled diodes were randomly selected for I-V and reverse breakdown characterizations. The crystal orientation of the β -Ga₂O₃ epi was illustrated. (b) The schematic illustration of the vertical layer structure and (c) a detailed view of an individual Si/ β -Ga₂O₃ p-n diode.

Figure 4(a) depicts the measured I-V characteristics of randomly selected (see Figure 3(a) for the device labeling) Si/ β -Ga₂O₃ p-n diodes in the range of -2 to 2 V. From an I-V measurement survey of the p-n diodes over an area of about $1 \times 1 \text{ mm}^2$, the yield of the working device is estimated to be 86%. The

ideality factors (n) of the Si/ β -Ga₂O₃ p-n diodes shown in Figure 4(a) were calculated and listed in Table 1. According to the equation of n as a function of interface defect density (D_{it}) in grafted heterojunction p-n diodes [45] and the interfacial layer thickness of 2.5 nm (to be described later), the D_{it} values of the Si/ β -Ga₂O₃ interface are estimated to be $1-3 \times 10^{12}$ /cm²·eV, considering that the interface dielectric constant may be any value in the range of 3.9 (SiO₂ [8]) to 10.43 (β -Ga₂O₃ [9]). The D_{it} value is lower than that of the Si/ β -Ga₂O₃ n-n diode fabricated by SAB [52]. As shown in Figure 4(a), the ultralow reverse current also indicates a very low density of generation centers at the grafted Si/ β -Ga₂O₃ interface, making the grafted Si/ β -Ga₂O₃ p-n diodes ideal for applications such as high-power devices and photo detectors, etc. Figure 4(b) further shows the measured breakdown characteristics of a few randomly selected devices (see Figure 3(a)). The breakdown ranges from 20-25 V (Table 2). This variation is because the avalanche phenomenon is a stochastic process.

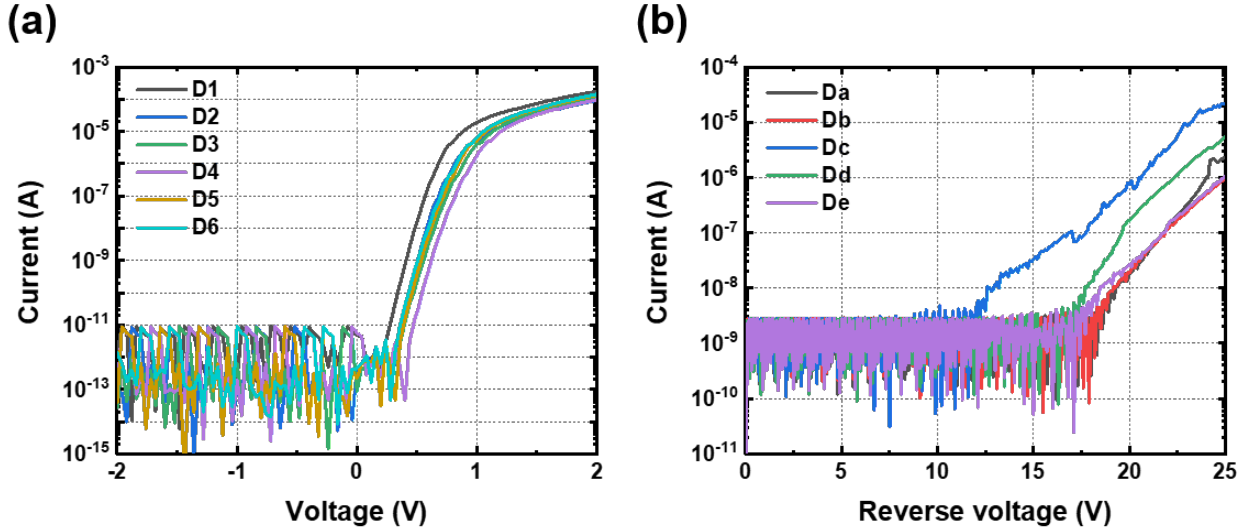


Figure 4. (a) I-V characteristics obtained from randomly selected Si/ β -Ga₂O₃ p-n diodes in the range of \pm 2 V. (b) Measured reverse I-V and breakdown characteristics of a few randomly selected Si/ β -Ga₂O₃ p-n diodes.

Table 1. Summary of the ideality factor (n) of randomly selected Si/ β -Ga₂O₃ p-n diodes.

Device #	D1	D2	D3	D4	D5	D6
n	1.13	1.17	1.36	1.26	1.24	1.22

Table 2. Summary of the breakdown voltage (BV) of randomly selected Si/ β -Ga₂O₃ p-n diodes.

Device #	Da	Db	Dc	Dd	De
BV (V)	24.2	25	20.7	22.4	24.9

The measured C-V characteristics of the Si/ β -Ga₂O₃ p-n diodes are shown in Figure 5. Little frequency dispersion was observed in the C-V curves in a frequency range of 10 kHz to 2 MHz (Figure 5(a) and 5(b)). The p-n junction capacitance values only vary with the reverse bias values that were applied to the diodes. The non-dispersion of the C-V curves indicates that a Si/ β -Ga₂O₃ interface of high quality and low D_{it} was attained. To estimate the upper values of the D_{it} based on the C-V curves, Silvaco Atlas simulations of the Si/ β -Ga₂O₃ p-n diode structure (Figure 3(b)) with different D_{it} values were performed. The simulation results are shown in Figure 5(c). As can be seen, without significant change of capacitance within the given frequency range, the upper value of the D_{it} is $6 \times 10^{12} / \text{cm}^2 \cdot \text{eV}$, in agreement with the I-V measurement results.

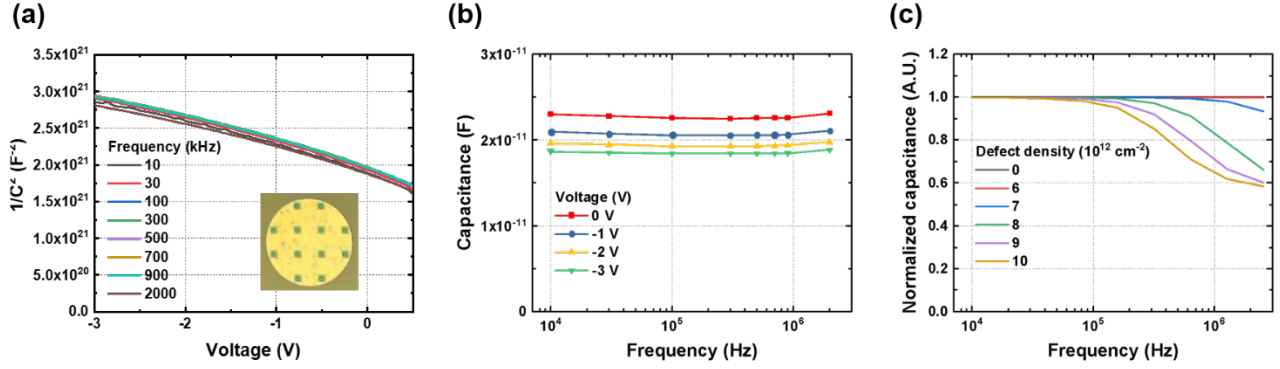


Figure 5. (a) Measured $1/C^2$ of the Si/ β -Ga₂O₃ p-n diode as a function of bias voltage at multiple frequencies from 10 kHz to 2 MHz. The inset is the optical image of the C-V diode, which has a larger anode area. (b) Plot of the junction capacitance of the identical Si/ β -Ga₂O₃ p-n diode in (a) as function of measurement frequency under different bias values from 0 to -3 V, showing that the diode junction capacitance only varies with the bias. (c) The simulated C-V plots of the Si/ β -Ga₂O₃ p-n diode under 0 V with different interface D_{it} values.

Considering the low D_{it} values attained at the Si/ β -Ga₂O₃ p-n junction, the Fermi level pinning due to charge traps at the grafted Si/ β -Ga₂O₃ interface is expected to be negligible. Therefore, the band alignment between the Si and the β -Ga₂O₃ is expected to follow the electron affinity rule. Since the electron affinity of β -Ga₂O₃ is 4.00 eV [53], the Si/ β -Ga₂O₃ p-n junction alignment can be constructed as shown in Figure 6. The Fermi energy level of the Si and that of the β -Ga₂O₃ were calculated according to the parameters shown in Fig. 3(b). Such an ideal band alignment can only be possible if the interface D_{it} is sufficiently low [45]. It is noted that such a type-I band alignment between Si and β -Ga₂O₃ would be much more beneficial for future development of triode bipolar junction transistors than other β -Ga₂O₃-based pn junctions that employ the p-type oxides [20, 21, 23].

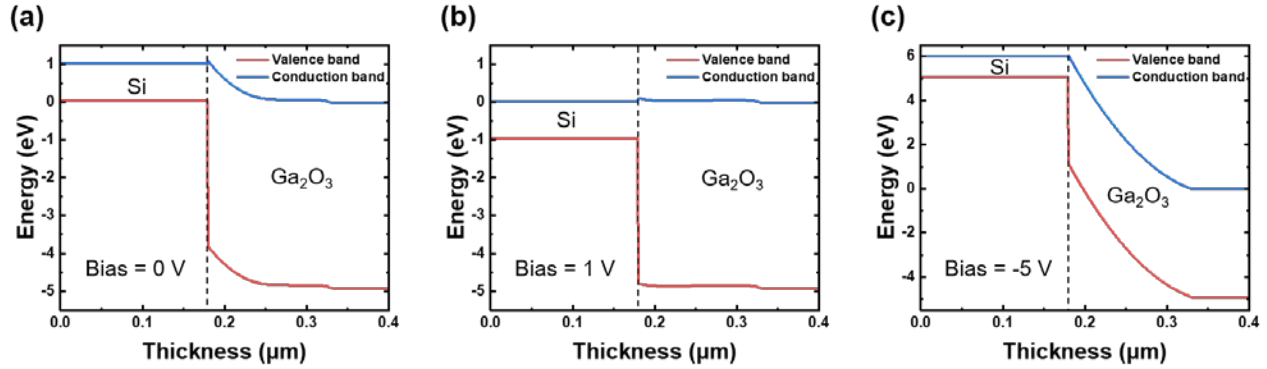


Figure 6. Constructed Si/ β -Ga₂O₃ p-n junction band diagram under (a) equilibrium (0 V), (b) forward bias of 1.0 V, and (c) reverse bias of -5 V.

Figure 7(a) shows the drawing about the relative orientation of the monocrystalline Si and β -Ga₂O₃ of the characterized Si/ β -Ga₂O₃ p-n diode. Figure 7(b) shows the overview (or low magnification) HAADF image of the grafted Si/ β -Ga₂O₃ interface. The high-resolution (HR)-HAADF images viewed along two different lateral directions (Figure 7(c) and 7(d)) clearly show the β -Ga₂O₃ lattice structure along the [201] axis and the Si lattice structure along the [101] axis, respectively. The interfacial amorphous layer is estimated to be only ~2.0-2.5 nm thick. The thin interface layer (SiGaO_x) is expected to facilitate charge carrier transport through the interface. The small mis-orientation angle between the Si [101] and the β -Ga₂O₃ [201] axes was caused by “misalignment” during processes such as SOI wafer dicing and possibly during the Si membrane transfer. The mis-orientation however does not have any adverse effects on the device performance since the interface layer between Si and β -Ga₂O₃ is amorphous. In fact, the alignment applied when transferring Si membrane to β -Ga₂O₃ was merely for the ease of photolithography steps. No accurate alignment was needed or enforced during the Si membrane transfer.

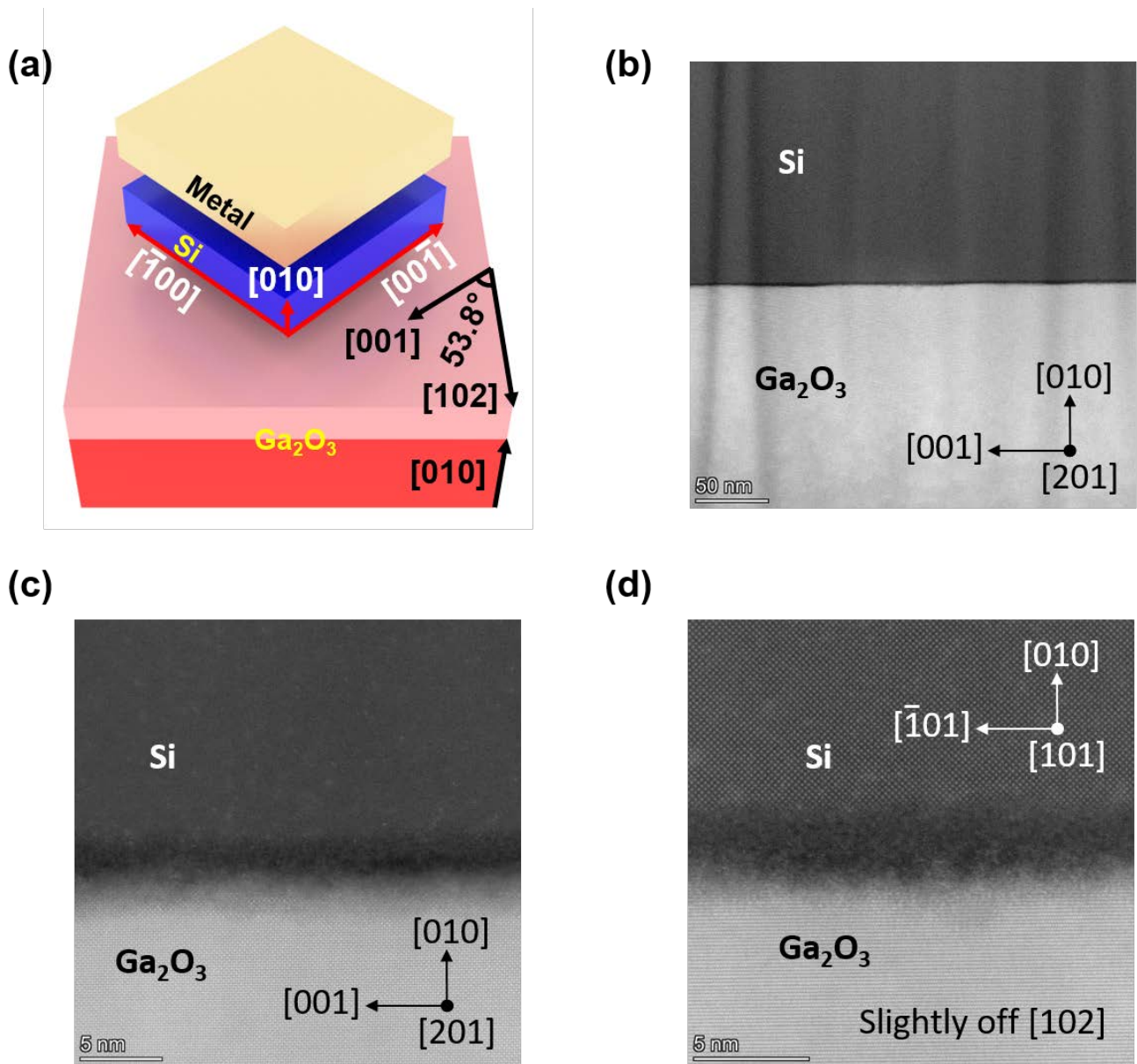


Figure 7. STEM imaging of the Si/ β -Ga₂O₃ grafted interface. (a) Illustration of crystalline orientations of the characterized functional Si/ β -Ga₂O₃ p-n diode. (b) A HAADF image of the Si/ β -Ga₂O₃ interface. (c) and (d) HR-HAADF images showing the cross-sectional view of the Si/ β -Ga₂O₃ interface with different viewing angles to show the lattice structure of the β -Ga₂O₃ and the Si, respectively.

Figure 8(a) shows the EELS scanning area of the Si/ β -Ga₂O₃ interface for identifying the elements distribution, viewed along Si [101] axis and slightly off β -Ga₂O₃ [102] axis. Figures 8(b)-(e) show the

false-color element distributions of Si, Ga, O, and C atoms across the interface and Figure 8(f) shows the overlay of all above distributions. By comparing the Si (Figure 8(b)) and the Ga (Figure 8(c)) distributions, Si and Ga are not intermixed. The clear physical separation of the Si atoms and the Ga atoms is critical in reducing the value of D_{it} at the interface. Figure 8(d) indicates the presence of oxygen atoms at the interface. It is speculated that the oxygen atoms at the surface of the β -Ga₂O₃ reacted with the surface Si atoms during the thermal annealing process. This Si-O reaction passivates the surface dangling bonds of the monocrystalline Si. Combined with the self-passivation effect of the β -Ga₂O₃ surface, a substantially low D_{it} value at the Si/ β -Ga₂O₃ interface was obtained, as shown in I-V and C-V measurements. From the analysis, sufficient oxygen atom presence at the surface of β -Ga₂O₃ is essential to achieve adequate surface passivation of the Si surface, which perhaps also be advantageous for further improved surface passivation of β -Ga₂O₃. Figure 8(e) shows the presence of some C atoms at the interface, which was unexpected. However, by XPS analysis (to be detailed below), it was confirmed that C atoms were highly possibly from isopropyl alcohol (IPA) residue during the Si NM release process (Figure 10(b)). Furthermore, the effects C atoms on the Si/ β -Ga₂O₃ p-n diode characteristics are unknown.

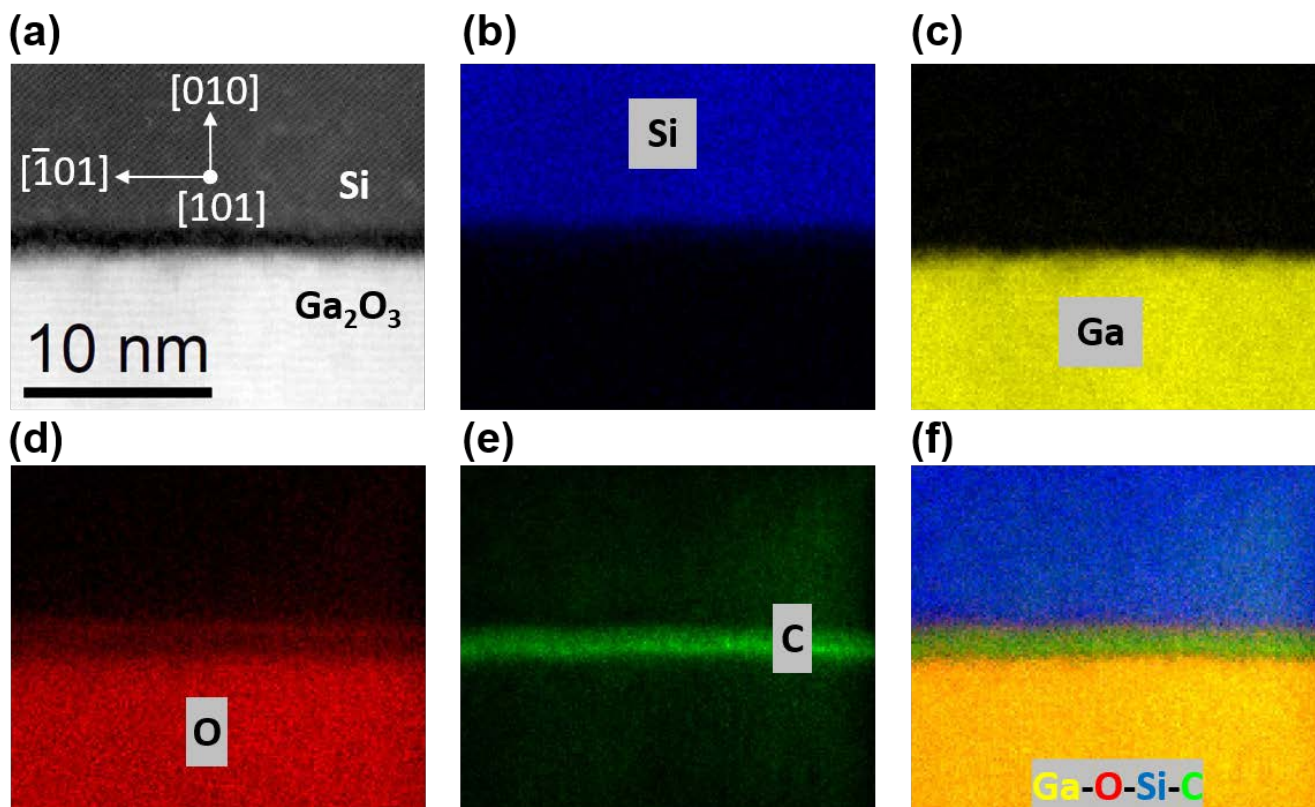


Figure 8. EELS elemental mapping at the Si/ β -Ga₂O₃ interface. (a) The scanning region of the EELS mapping. (b)-(e) The fake color images showing the distributions of the element Si, Ga, O and C, respectively. (f) Overlaid distribution of Ga-O-Si-C elements at the interface.

As discussed above, the oxygen atoms at the interface of Si/ β -Ga₂O₃ play the central role in achieving double side passivation of the two materials. To better understand the role of oxygen atoms on the surface of the β -Ga₂O₃ epi sample during its surface preparations, and particularly to understand how ion bombarding (*e.g.*, used in surface preparation in SAB) can affect β -Ga₂O₃ surface oxygen atoms, the XPS analysis results on the O 1s, Ga 3d, and C 1s spectra were illustrated in Figure 9. The measurements were taken from the β -Ga₂O₃ epi sample under three different surface conditions. The XPS measurement was first taken on the “grafting ready” sample, followed by two iterations of a 30-s Ar ion in-situ etching and an XPS measurement on the same sample. During the XPS spectra collection, auto-height process of

the sample stage inside the XPS chamber was imitated at the beginning of the experiment. Hence, the absolute intensity of the spectra collected under the three surface conditions can be compared quantitatively. As clearly shown in Figure 9(a), the surface oxygen atom concentration has been reduced substantially (~5% reduction in peak area) by the first 30-s Ar ion etching. Since the Ar etching is typically used in a SAB process, the degradation of surface passivation due to the removal of the surface oxygen atoms should be inevitable. In our work, the enrichment of surface O atoms due to the soaking process of the β -Ga₂O₃ sample in the Piranha solution becomes the key step (opposing the surface treatments in SAB) to achieve adequate surface passivation for Si and β -Ga₂O₃. On the other hand, the concentration of surface Ga atoms increased (~3-4% increase in peak area) after the first 30-s Ar etching (Figure 4(b)). Furthermore, no significant change in XPS spectra was observed between the 30-s Ar-etched sample and the 60-s Ar-etched sample, indicating that the observed difference in Ga and O concentration only exists in a nanometer-scale surface layer and is not caused by the potential difference in sputtering rate between Ga and O atoms but real. Both Figure 9(a) and 9(b) indicate that 30-sec Ar ion etching is long enough to modify the surface of the “grafting ready” sample surface. Additional Ar ion beam etching does not induce further changes in the stoichiometry of the surface of the β -Ga₂O₃. Figure 9(c) shows that there was no carbon residue on the surface of the β -Ga₂O₃ sample (to the instrumental resolution limit of the XPS), which confirmed that the C source was from the Si side (*i.e.*, IPA). The XPS spectra suggests that there exists an ultrathin oxygen-rich layer on the surface of the β -Ga₂O₃ substrate. The oxygen atoms in this layer reacted with the surface atoms of the Si layer forming the final interface layer (~2-2.5 nm) that serve as the quantum tunneling the double-side passivation interface between the two monocrystalline crystals: the Si and the β -Ga₂O₃. The role of the interface SiGaO_x has served the identical roles in other grafted heterostructures where an ultrathin Al₂O₃ layer was applied using atomic layer deposition (ALD) [45, 54-61].

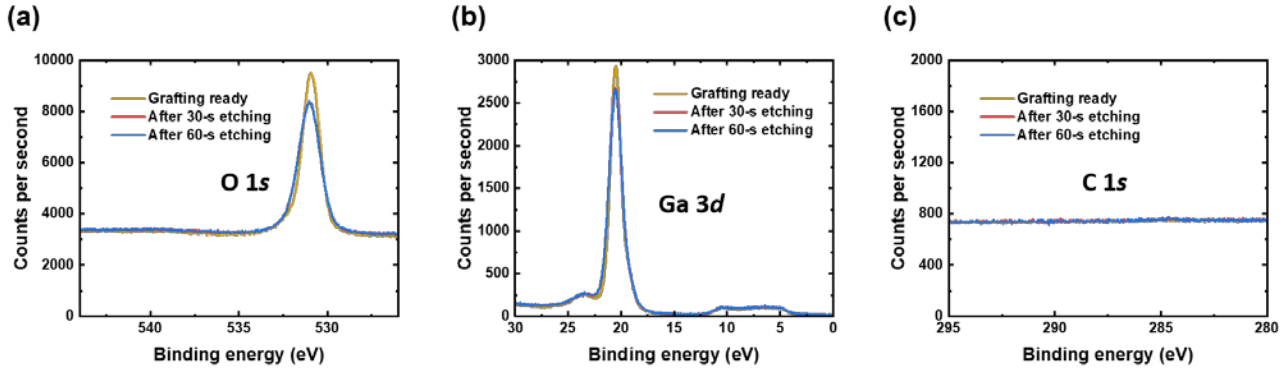


Figure 9. (a) Ga 3d, (b) O 1s, and (c) C 1s XPS spectra collected on the β -Ga₂O₃ epi sample under different surface conditions. The gold color spectra were collected from the “grafting ready” sample and the red color and the blue color spectra were collected after a 30-s and another 30-s ion-gun etching.

3. Conclusions

In this work, we applied the semiconductor grafting approach to fabricate Si/ β -Ga₂O₃ p-n diodes for the first time. With enhanced concentration of oxygen atoms at the interface of Si/ β -Ga₂O₃, sufficient double side surface passivation was achieved for both Si and β -Ga₂O₃ with a D_{it} value of $1-3 \times 10^{12}$ /cm²·eV. By controlling the thermal budget during the chemical bonding formation process, ~2-2.5 nm interface amorphous layer was attained without inducing Ga and Si atoms inter-diffusion, verified by STEM imaging, to ensure effective quantum tunneling. A diode array with high fabrication yield was demonstrated along with a p-n diode rectification of 1.3×10^7 at ± 2 V, a diode ideality factor as low as 1.13 and avalanche reverse breakdown characteristics. The dispersion-free C-V versus frequency of the Si/ β -Ga₂O₃ p-n junction confirmed the low D_{it} results from the grafting approach. The near-ideal Si/ β -Ga₂O₃ heterojunction formed in this work, the grafting approach being applied to combine single crystal Si as the p-type semiconductors with the n-type β -Ga₂O₃, and the membrane transfer printing method used in lieu of bulk Si (or SOI) all could be further expanded to the future development of β -Ga₂O₃-based transistors.

4. Experiment Section

Epitaxy growth of β -Ga₂O₃

Epitaxy growth of β -Ga₂O₃ and cleaning prior diode fabrication. The β -Ga₂O₃ epitaxial structure consists of ~150 nm thick lightly Si doped ($\sim 2 \times 10^{17} \text{ cm}^{-3}$) homoepitaxial layer grown using Agnitron Technology's Agilis 500 MOCVD reactor [4-6] on a Sn-doped ($\sim 5 \times 10^{18} \text{ cm}^{-3}$) (010) β -Ga₂O₃ substrate (Novel Crystal Technology) of ~550 μm . (Fig. 1(a) and 1(b)). Trimethylgallium (TMGa), pure oxygen (5N), and silane diluted in nitrogen (SiH₄/N₂) were used as precursors and argon (5N) as carrier gas during the growth. The Ar and O₂ gases were passed through point-of-use purifiers to reduce the impurity level to <1 ppm. Prior to loading the sample into the growth chamber, the substrate was cleaned using hydrofluoric acid (HF) for 30 minutes. The as-grown β -Ga₂O₃ epi sample was characterized by X-ray diffraction (XRD) and the surface roughness of the n-side surface of the β -Ga₂O₃ was characterized by atomic force microscope (AFM).

Characterization of β -Ga₂O₃ substrate

The as-grown β -Ga₂O₃ substrate was first dipped into acetone and sonicated for ten minutes, and the same process was repeated using isopropyl alcohol (IPA). After that, the substrate was put into Piranha solution (96% H₂SO₄ : H₂O₂ = 3:1) for ten minutes at room temperature. Then, the samples were thoroughly rinsed with deionized (DI) water for one minute. With this step, it is expected to enrich the oxygen atoms at the surface of the β -Ga₂O₃ substrate considering that oxygen atoms provide passivation function at the interface between Si and β -Ga₂O₃. The same cleaning procedures were iterated with RCA1 solution (29% NH₄OH : 30% H₂O₂ : DI water = 1:1:5) and RCA2 solution (37% HCl : DI water = 1:1) in sequence, the sample was dipped into a diluted HF solution (49% HF : DI water = 1:20) for one minute. This sample was named the "grafting-ready" sample.

The grafting-ready sample was performed using a Thermo Scientific K Alpha X-ray Photoelectron Spectrometer (XPS) with Al K_{α} X-ray source ($h\nu = 1486.6$ eV). The sample was carried in a zip-bag filled with N_2 during the transportation from the lab to the XPS instrument to minimize the influence of air. It took about 10 min from moving the sample out of the HF solution to loading it into the XPS chamber. The instrument was calibrated by Au $4f_{7/2}$ peak at 84.0 eV. The following settings were applied to the spectrometer: 10 eV pass energy, 400 μm spot size, 5 s dwell time, and 0.05 eV step size. The auto-height of the sample stage was done only once at the start of the experiment. The Ga $3d$, O $1s$, and C $1s$ peaks were measured to collect the first set of data. The second set of data was obtained following a 30-s ion gun etching with 1 keV ion energy and a 2 mm raster size. And the third set of data was collected after another 30-s ion-gun etching.

Fabrication of transferable p+ Si membranes

To prepare Si membranes, a 6-inch Soitec^(R) p-type (14-22 $\Omega\cdot\text{cm}$) silicon (100)-on-insulator (SOI) substrate was used to begin with. The 8-inch SOI substrate has a 205 nm Si device layer and a 400 nm buried oxide (BOX) layer. A thermal oxidation process using a furnace tube under 1050 $^{\circ}\text{C}$ was applied to the SOI substrate for 12 min to grow 36 nm thick screen oxide. Then the SOI substrate was boron implanted at room temperature with a dose of 3×10^{15} cm^{-2} under 15 keV at an incident angle of 7° . After finishing the ion implantation, a thermal activation process at 950 $^{\circ}\text{C}$ for 40 min was performed using the same furnace tube. After finishing the activation process, the resultant Si device layer has a final thickness of 180-185 nm thick and a boron doping concentration ranging from 9.7×10^{19} cm^{-3} at its top surface to 9.5×10^{19} cm^{-3} at the bottom (next to the BOX layer), and the final top screen oxide become ~ 52 nm thick. All the above process conditions were guided with Silvaco Athena simulations, and after the dopant activation process the p+ Si device layer maintains its monocrystalline properties.

To fabricate Si membranes, the p+ SOI substrate was diced into 5-mm-by-5-mm squares. The size of dicing was to match the size of the β -Ga₂O₃ substrate used in this study. First, the top 52 nm thick screen oxide layer of the diced SOI squares was first removed by buffered oxide etchant solution. After that, a conventional photolithography process was performed to form a 9- μ m-by-9- μ m square-hole array pattern on the p+ Si device layer (Figure 10(a)). The holes were dry etched through the p+ Si layer using a SAMCO RIE-10NR Reactive Ion Etching (RIE) System. After removing the photoresist, the patterned SOI sample was dipped inside 49% HF for 3.5 hours to remove the BOX layer. The sample was then transferred to IPA solution, followed by transferring into DI water for 1 min each to completely rinse off HF. After drying up the DI water with N₂ air gun blow, the p+ Si membrane is ready for transfer printing for the Si/ β -Ga₂O₃ p-n diode fabrication (Figure 10(b)).

Fabrication of Si/ β -Ga₂O₃ heterostructure p-n diodes

The p-n diode fabrication process flow was depicted in Figure 10. The grafting-ready sample (Figure 10(c)) was metallized to form a cathode contact on the backside by depositing Ti/Au/Cu/Au (10/5/100/10 nm) metal stack using e-beam evaporation followed by rapid thermal annealing (RTA) at 600 °C for 10 s to form ohmic contacts (Figure 10(d)).

The p+ Si membrane sitting on the Si handling substrate was picked up using a polydimethylsiloxane (PDMS) stamp of a thickness of ~ 10 μ m. The stamp was fabricated from a mixture of monomer and crosslinker of ratio 4:1 and cured under 60 °C for 4 hours after a quick degassing process (Figure 10(e)). The p+ Si membrane was then transferred to the β -Ga₂O₃ substrate [62, 63]. The Si membrane transfer and printing process was performed in the ambient environment because oxygen atoms are considered beneficial to the desired double-side passivation as mentioned above. Due to the superior compliance of the Si membrane, an intimate contact can form without air trapped between the Si and β -Ga₂O₃ epi layer. Therefore, van der Waals bonding between Si membrane and the β -Ga₂O₃ epi substrate

can be uniformly created. Then the weak van der Waals bonding was converted into strong chemical bonding by RTA at 350 °C for 5 min in a N₂ environment (Figure 10(f)). XRD and Raman spectroscopy measurements were carried out on this Si/ β-Ga₂O₃ stack, by a Malvern Panalytical Empyrean X-ray diffractometer with a Cu K-α X-ray source and a Horiba LabRAM HR Evolution Raman spectrometer using a 532-nm laser respectively.

Another conventional photolithography was used to cast anode contact pattern on the transferred p+ Si layer, and then an e-beam deposition of Ni/Au/Cu/Au (10/5/100/10 nm) metal stack was followed to perform lift-off process (Figure 10(g)). The individual Si/Ga₂O₃ pn diodes were isolated from each other by etching away the exposed Si through RIE (Figure 10(h)), with the anode metal as the self-aligned etching masks. The anode area for each p-n diode after isolation is 37 × 37 μm². A thermal annealing of 600 °C for 10 seconds was performed on the isolated Si/Ga₂O₃ pn diode array to improve the ohmic contacts of both anodes and cathodes. For capacitance-voltage (C-V) voltage characterizations, larger anode area Si/β-Ga₂O₃ p-n diodes of round shape with an area of 2.79 × 10⁴ μm² were fabricated using the same fabrication process. The larger device area is to increase the diodes junction capacitance and to reduce the relative uncertainty of the capacitance measurements.

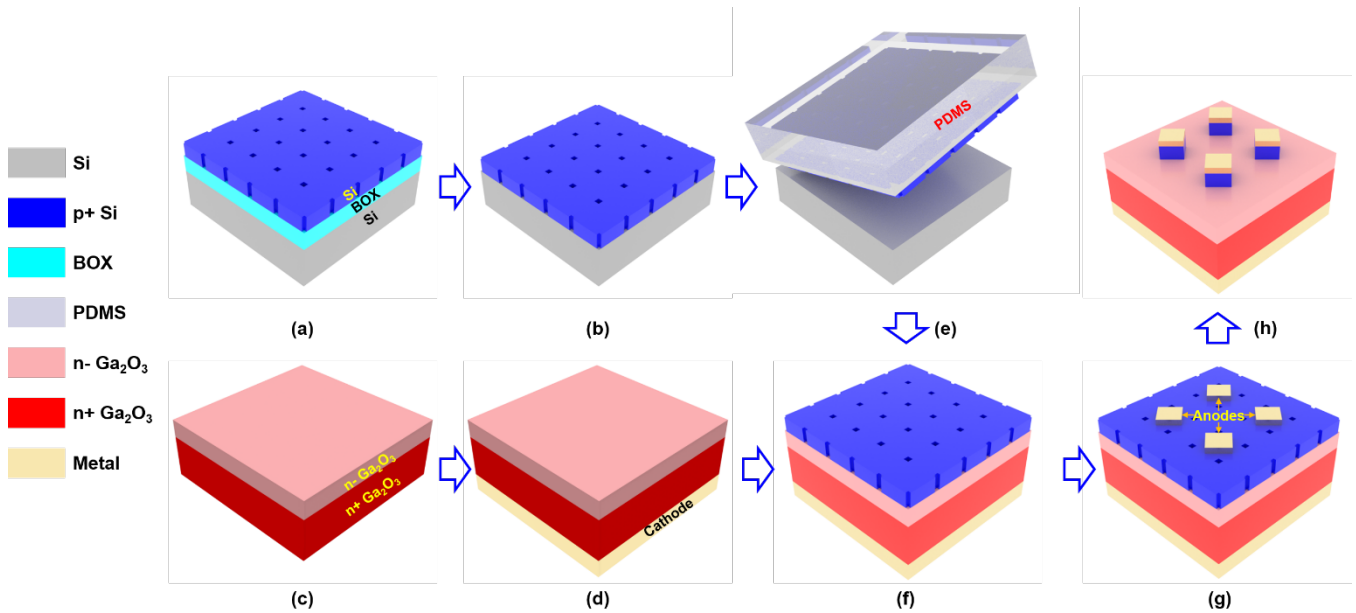


Figure 10. Illustration of fabrication process flow of the Si/Ga₂O₃ p-n diode. (a) RIE etching release holes on p+ Si device layer. (b) Release the p+ Si device layer using HF. (c) Surface preparation of the Ga₂O₃ epi. (d) Bottom cathode formation on the Ga₂O₃ epi. (e) Pick up of p+ Si membrane using a PDMS stamp. (f) Transfer-printing of the p+ Si membrane to the receiver Ga₂O₃ substrate. (g) Anode contact formation on the p+ Si layer. (h) Si/Ga₂O₃ pn diodes isolation and contacts ohmic thermal annealing.

I-V and C-V characterizations

The I-V and C-V of the Si/ β -Ga₂O₃ p-n diodes were measured by a Keithley 4200 semiconductor characterization system. The device reverse breakdown characteristics were measured using HP 4155B semiconductor parameter analyzer.

Si/ β -Ga₂O₃ interface imaging

The transmission electron microscopy (TEM) lamella, which was taken from an I-V characterized and functional Si/Ga₂O₃ pn diode, was prepared using a Thermo Fisher Scientific (TFS) Helios G4 dual-beam focused ion beam (FIB) system equipped with an EasyLift manipulator for the transfer of the lamella

to the Omniprobe FIB grid. To protect the surface morphology of the device, the electron beam-assisted carbon (C) and Pt deposition, followed by the Ga ion beam assisted Pt deposition were performed prior to the Ga ion milling. 30 kV Ga ion milling was used for the bulk milling, followed by 5 kV and 2 kV Ga ion milling, *i.e.*, low kV cleaning, to remove the damaged layer created by the 30 kV Ga ion milling.

Scanning transmission electron microscopy (STEM) micrographs were acquired using a Thermo Fisher Scientific (TFS) Themis Z aberration-corrected electron microscope operated at 300 keV. The convergence semi-angle of 21 mrad and the collection semi-angle of 70-200 mrad were used for the high angle annular dark-field (HAADF) image acquisition. Electron energy loss spectroscopy (EELS) analysis was performed using a Gatan Continuum electron energy loss spectrometer and image filter and K3 electron direct detector. The collection semi-angle of 50 mrad was used to acquire the EELS spectra.

Acknowledgements

The work was supported by a CRG grant (2022-CRG11-5079.2) by the King Abdullah University of Science and Technology (KAUST).

Conflict of Interest

The authors declare no conflict of interest.

Data Availability Statement

The data that support the findings of this study are available from the corresponding authors upon reasonable request.

Keywords

semiconductor grafting, Gallium oxide, heterojunction, diodes, scanning transmission electron microscopy, monocrystalline membrane, transfer-printing, ultra-wide bandgap (UWBG), X-ray photoelectron spectroscopy, Raman spectroscopy

References

- [1] M. Higashiwaki *et al.*, "Recent progress in Ga₂O₃ power devices," *Semiconductor Science and Technology*, vol. 31, no. 3, p. 034001, 2016.
- [2] J. Tsao *et al.*, "Ultrawide-bandgap semiconductors: research opportunities and challenges," *Advanced Electronic Materials*, vol. 4, no. 1, p. 1600501, 2018.
- [3] C. Janowitz *et al.*, "Experimental electronic structure of In₂O₃ and Ga₂O₃," *New Journal of Physics*, vol. 13, no. 8, p. 085014, 2011.
- [4] F. Alema *et al.*, "Low temperature electron mobility exceeding 104 cm²/V s in MOCVD grown β -Ga₂O₃," *APL Materials*, vol. 7, no. 12, p. 121110, 2019.
- [5] F. Alema *et al.*, "Low 1.0 \times 10¹⁴ cm⁻³ free carrier concentration in epitaxial β -Ga₂O₃ grown by MOCVD," *APL Materials*, vol. 8, no. 2, p. 021110, 2020.
- [6] G. Seryogin *et al.*, "MOCVD growth of high purity Ga₂O₃ epitaxial films using trimethylgallium precursor," *Applied Physics Letters*, vol. 117, no. 26, p. 262101, 2020.
- [7] K. Sasaki, A. Kuramata, T. Masui, E. G. Villora, K. Shimamura, and S. Yamakoshi, "Device-quality β -Ga₂O₃ epitaxial films fabricated by ozone molecular beam epitaxy," *Applied Physics Express*, vol. 5, no. 3, p. 035502, 2012.
- [8] K. Sasaki, M. Higashiwaki, A. Kuramata, T. Masui, and S. Yamakoshi, "MBE grown Ga₂O₃ and its power device applications," *Journal of Crystal Growth*, vol. 378, pp. 591-595, 2013.
- [9] H. Murakami *et al.*, "Homoepitaxial growth of β -Ga₂O₃ layers by halide vapor phase epitaxy," *Applied Physics Express*, vol. 8, no. 1, p. 015503, 2014.

- [10] M. Higashiwaki *et al.*, "Ga₂O₃ Schottky barrier diodes with n-Ga₂O₃ drift layers grown by HVPE," in *2015 73rd Annual Device Research Conference (DRC)*, 2015: IEEE, pp. 29-30.
- [11] J. Yang, S. Ahn, F. Ren, S. Pearton, S. Jang, and A. Kuramata, "High breakdown voltage (β -Ga₂O₃ Schottky rectifiers," *IEEE Electron Device Letters*, vol. 38, no. 7, pp. 906-909, 2017.
- [12] J. Yang, F. Ren, M. Tadjer, S. Pearton, and A. Kuramata, "2300V reverse breakdown voltage Ga₂O₃ Schottky rectifiers," *ECS Journal of Solid State Science and Technology*, vol. 7, no. 5, p. Q92, 2018.
- [13] W. Li, D. Saraswat, Y. Long, K. Nomoto, D. Jena, and H. G. Xing, "Near-ideal reverse leakage current and practical maximum electric field in β -Ga₂O₃ Schottky barrier diodes," *Applied Physics Letters*, vol. 116, no. 19, p. 192101, 2020.
- [14] H. Zhou, M. Si, S. Alghamdi, G. Qiu, L. Yang, and D. Y. Peide, "High-Performance Depletion/Enhancement-mode β -Ga₂O₃ on Insulator (GOOI) Field-Effect Transistors With Record Drain Currents of 600/450 mA/mm," *IEEE Electron Device Letters*, vol. 38, no. 1, pp. 103-106, 2016.
- [15] H. Zhou, K. Maize, G. Qiu, A. Shakouri, and P. D. Ye, " β -Ga₂O₃ on insulator field-effect transistors with drain currents exceeding 1.5 A/mm and their self-heating effect," *Applied Physics Letters*, vol. 111, no. 9, p. 092102, 2017.
- [16] Z. Hu *et al.*, "Enhancement-mode Ga₂O₃ vertical transistors with breakdown voltage > 1 kV," *IEEE Electron Device Letters*, vol. 39, no. 6, pp. 869-872, 2018.
- [17] H. Dong *et al.*, "Progress of power field effect transistor based on ultra-wide bandgap Ga₂O₃ semiconductor material," *Journal of Semiconductors*, vol. 40, no. 1, p. 011802, 2019.

- [18] Z. Jiang *et al.*, "P-type β -Ga₂O₃ metal-semiconductor-metal solar-blind photodetectors with extremely high responsivity and gain-bandwidth product," *Materials Today Physics*, vol. 14, p. 100226, 2020.
- [19] C. Ma *et al.*, "Exploring the feasibility and conduction mechanisms of P-type nitrogen-doped β -Ga₂O₃ with high hole mobility," *Journal of Materials Chemistry C*, vol. 10, no. 17, pp. 6673-6681, 2022.
- [20] Y. Kokubun, S. Kubo, and S. Nakagomi, "All-oxide p–n heterojunction diodes comprising p-type NiO and n-type β -Ga₂O₃," *Applied Physics Express*, vol. 9, no. 9, p. 091101, 2016.
- [21] T. Watahiki, Y. Yuda, A. Furukawa, M. Yamamuka, Y. Takiguchi, and S. Miyajima, "Heterojunction p-Cu₂O/n-Ga₂O₃ diode with high breakdown voltage," *Applied Physics Letters*, vol. 111, no. 22, p. 222104, 2017.
- [22] M. Budde *et al.*, "SnO/ β -Ga₂O₃ vertical pn heterojunction diodes," *Applied Physics Letters*, vol. 117, no. 25, p. 252106, 2020.
- [23] J. Zhang *et al.*, "Ultra-wide bandgap semiconductor Ga₂O₃ power diodes," *Nature communications*, vol. 13, no. 1, p. 3900, 2022.
- [24] T. R. Chung, L. Yang, N. Hosoda, H. Takagi, and T. Suga, "Wafer direct bonding of compound semiconductors and silicon at room temperature by the surface activated bonding method," *Applied surface science*, vol. 117, pp. 808-812, 1997.
- [25] U. Gösele *et al.*, "Fundamental issues in wafer bonding," *Journal of Vacuum Science & Technology A: Vacuum, Surfaces, and Films*, vol. 17, no. 4, pp. 1145-1152, 1999.
- [26] P. Kopperschmidt and R. Scholz, "Interface defects in integrated hybrid semiconductors by wafer bonding," *Physica B: Condensed Matter*, vol. 308, pp. 1205-1208, 2001.

- [27] L. Dozsa, B. Szentpali, D. Pasquariello, and K. Hjort, "Point defects generated by direct-wafer bonding of silicon," *Journal of electronic materials*, vol. 31, no. 2, pp. 113-118, 2002.
- [28] D. Pasquariello and K. Hjort, "Plasma-assisted InP-to-Si low temperature wafer bonding," *IEEE Journal of Selected Topics in Quantum Electronics*, vol. 8, no. 1, pp. 118-131, 2002.
- [29] C. Lian, H. Xing, C. S. Wang, L. McCarthy, and D. Brown, "DC characteristics of AlGaAs/GaAs/GaN HBTs formed by direct wafer fusion," *IEEE electron device letters*, vol. 28, no. 1, pp. 8-10, 2006.
- [30] C. Lian, H. G. Xing, C. S. Wang, D. Brown, and L. McCarthy, "Gain degradation mechanisms in wafer fused Al Ga As/ Ga As/ Ga N heterojunction bipolar transistors," *Applied Physics Letters*, vol. 91, no. 6, p. 063502, 2007.
- [31] C. Lian, H. G. Xing, Y.-C. Chang, and N. Fichtenbaum, "Electrical transport properties of wafer-fused p-GaAs/n-GaN heterojunctions," *Applied Physics Letters*, vol. 93, no. 11, p. 112103, 2008.
- [32] H. Moriceau *et al.*, "Overview of recent direct wafer bonding advances and applications," *Advances in Natural Sciences: Nanoscience and Nanotechnology*, vol. 1, no. 4, p. 043004, 2011.
- [33] F. Gity *et al.*, "Characterization of germanium/silicon p-n junction fabricated by low temperature direct wafer bonding and layer exfoliation," *Applied Physics Letters*, vol. 100, no. 9, p. 092102, 2012.
- [34] K. Tanabe, K. Watanabe, and Y. Arakawa, "III-V/Si hybrid photonic devices by direct fusion bonding," *Scientific reports*, vol. 2, p. 349, 2012.
- [35] F. Gity *et al.*, "Ge/Si heterojunction photodiodes fabricated by low temperature wafer bonding," *Optics express*, vol. 21, no. 14, pp. 17309-17314, 2013.
- [36] K. Derendorf *et al.*, "Fabrication of GaInP/GaAs//Si solar cells by surface activated direct wafer bonding," *IEEE Journal of Photovoltaics*, vol. 3, no. 4, pp. 1423-1428, 2013.

- [37] C.-K. Tseng *et al.*, "A self-assembled microbonded germanium/silicon heterojunction photodiode for 25 Gb/s high-speed optical interconnects," *Scientific reports*, vol. 3, p. 3225, 2013.
- [38] F. Dimroth *et al.*, "Comparison of direct growth and wafer bonding for the fabrication of GaInP/GaAs dual-junction solar cells on silicon," *IEEE Journal of Photovoltaics*, vol. 4, no. 2, pp. 620-625, 2014.
- [39] J. Kim, M. A. Laurent, H. Li, S. Lal, and U. K. Mishra, "Barrier reduction via implementation of InGaN interlayer in wafer-bonded current aperture vertical electron transistors consisting of InGaAs channel and N-polar GaN drain," *Applied Physics Letters*, vol. 106, no. 2, p. 023506, 2015.
- [40] J. Liang, L. Chai, S. Nishida, M. Morimoto, and N. Shigekawa, "Investigation on the interface resistance of Si/GaAs heterojunctions fabricated by surface-activated bonding," *Japanese Journal of Applied Physics*, vol. 54, no. 3, p. 030211, 2015.
- [41] A. C. Tamboli *et al.*, "III-V/Si wafer bonding using transparent, conductive oxide interlayers," *Applied Physics Letters*, vol. 106, no. 26, p. 263904, 2015.
- [42] K. Xiong *et al.*, "AlGaAs/Si dual-junction tandem solar cells by epitaxial lift-off and print-transfer-assisted direct bonding," *Energy Science & Engineering*, vol. 6, no. 1, pp. 47-55, 2018.
- [43] N. Shigekawa *et al.*, "GaAs/indium tin oxide/Si bonding junctions for III-V-on-Si hybrid multijunction cells with low series resistance," *IEEE Journal of Photovoltaics*, vol. 8, no. 3, pp. 879-886, 2018.
- [44] P. Sittimart, S. Ohmagari, T. Matsumae, H. Umezawa, and T. Yoshitake, "Diamond/ β -Ga₂O₃ pn heterojunction diodes fabricated by low-temperature direct-bonding," *AIP Advances*, vol. 11, no. 10, p. 105114, 2021.
- [45] D. Liu *et al.*, "Lattice-mismatched semiconductor heterostructures," *arXiv preprint arXiv:1812.10225*, 2018/12/26 2018.

- [46] Y. Yao, R. Gangireddy, J. Kim, K. K. Das, R. F. Davis, and L. M. Porter, "Electrical behavior of β -Ga₂O₃ Schottky diodes with different Schottky metals," *Journal of Vacuum Science & Technology B, Nanotechnology and Microelectronics: Materials, Processing, Measurement, and Phenomena*, vol. 35, no. 3, p. 03D113, 2017.
- [47] E. Farzana, Z. Zhang, P. K. Paul, A. R. Arehart, and S. A. Ringel, "Influence of metal choice on (010) β -Ga₂O₃ Schottky diode properties," *Applied Physics Letters*, vol. 110, no. 20, p. 202102, 2017.
- [48] J. Liang *et al.*, "Fabrication of β -Ga₂O₃/Si heterointerface and characterization of interfacial structures for high-power device applications," *Japanese Journal of Applied Physics*, vol. 61, no. SF, p. SF1001, 2022.
- [49] Y. Okada and Y. Tokumaru, "Precise determination of lattice parameter and thermal expansion coefficient of silicon between 300 and 1500 K," *Journal of applied physics*, vol. 56, no. 2, pp. 314-320, 1984.
- [50] M. E. Liao *et al.*, "Coefficients of thermal expansion of single crystalline β -Ga₂O₃ and in-plane thermal strain calculations of various materials combinations with β -Ga₂O₃," *APL Materials*, vol. 7, no. 2, p. 022517, 2019.
- [51] J. Rogers, M. Lagally, and R. Nuzzo, "Synthesis, assembly and applications of semiconductor nanomembranes," *Nature*, vol. 477, no. 7362, pp. 45-53, 2011.
- [52] Z. Wang, D. Takatsuki, J. Liang, T. Kitada, N. Shigekawa, and M. Higashiwaki, "Fabrication of n-Si/n-Ga₂O₃ heterojunctions by surface-activated bonding and their electrical properties," *Journal of Applied Physics*, vol. 131, no. 7, p. 074501, 2022.

- [53] M. Mohamed, K. Irmscher, C. Janowitz, Z. Galazka, R. Manzke, and R. Fornari, "Schottky barrier height of Au on the transparent semiconducting oxide β -Ga₂O₃," *Applied Physics Letters*, vol. 101, no. 13, p. 132106, 2012.
- [54] D. Liu *et al.*, "229 nm UV LEDs on aluminum nitride single crystal substrates using p-type silicon for increased hole injection," *Applied Physics Letters*, vol. 112, no. 8, p. 081101, 2018.
- [55] D. Liu *et al.*, "226 nm AlGa_N/AlN UV LEDs using p-type Si for hole injection and UV reflection," *Applied Physics Letters*, vol. 113, no. 1, p. 011111, 2018.
- [56] S. J. Cho *et al.*, "P-type silicon as hole supplier for nitride-based UVC LEDs," *New Journal of Physics*, vol. 21, no. 2, p. 023011, 2019.
- [57] S. J. Cho *et al.*, "Fabrication of AlGaAs/GaAs/diamond heterojunctions for diamond-collector HBTs," *AIP Advances*, vol. 10, no. 12, p. 125226, 2020.
- [58] J. Gong *et al.*, "Influences of ALD Al₂O₃ on the surface band-bending of c-plane, Ga-face GaN," *Japanese Journal of Applied Physics*, vol. 61, no. 1, p. 011003, 2021.
- [59] J. Gong *et al.*, "Interfacial band parameters of ultrathin ALD–Al₂O₃, ALD–HfO₂, and PEALD–AlN/ALD–Al₂O₃ on c-plane, Ga-face GaN through XPS measurements," *Journal of Applied Physics*, vol. 132, no. 13, p. 135302, 2022.
- [60] J. Gong *et al.*, "Synthesis and Characteristics of Transferrable Single-Crystalline AlN Nanomembranes," *Advanced Electronic Materials*, vol. 9, no. 5, p. 2201309, 2023.
- [61] S. Qiu *et al.*, "Interfacial band parameters of ultrathin ALD-ZrO₂ on Ga-polar GaN through XPS measurements," *AIP Advances*, vol. 13, no. 5, 2023.
- [62] E. Menard, R. G. Nuzzo, and J. A. Rogers, "Bendable single crystal silicon thin film transistors formed by printing on plastic substrates," *Applied Physics Letters*, vol. 86, no. 9, p. 093507, 2005.

- [63] K. Zhang, J.-H. Seo, W. Zhou, and Z. Ma, "Fast flexible electronics using transferrable silicon nanomembranes," *Journal of Physics D: Applied Physics*, vol. 45, no. 14, p. 143001, 2012.

The preliminary results contained in the manuscript was presented as a poster in

The 5th US Gallium Oxide Workshop

Washington, D.C. USA

August 07-10, 2022

1. Introduction

(1) Why Ga₂O₃?

- High breakdown electrical field (8 MV/cm).
- High electron saturation velocity (1.1 × 10⁷ cm/s).
- Ultra-Wide Bandgap: 4.9 eV
- Available up to 4-inch wafers.

(2) Why no Ga₂O₃ bipolar devices? → Ineffective p-type doping in Ga₂O₃.

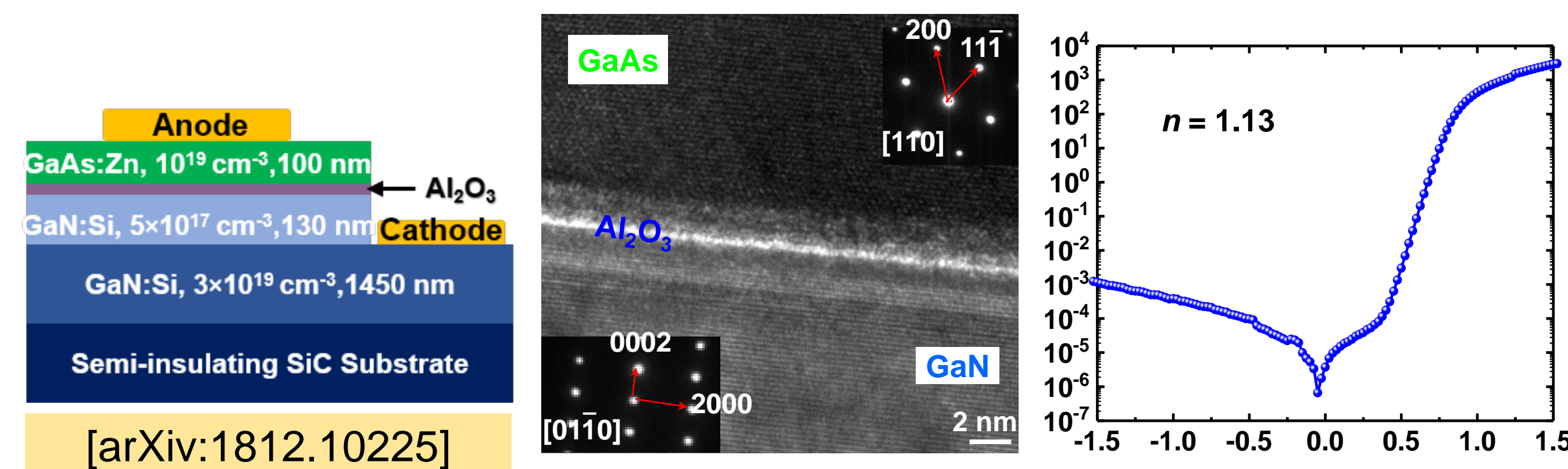
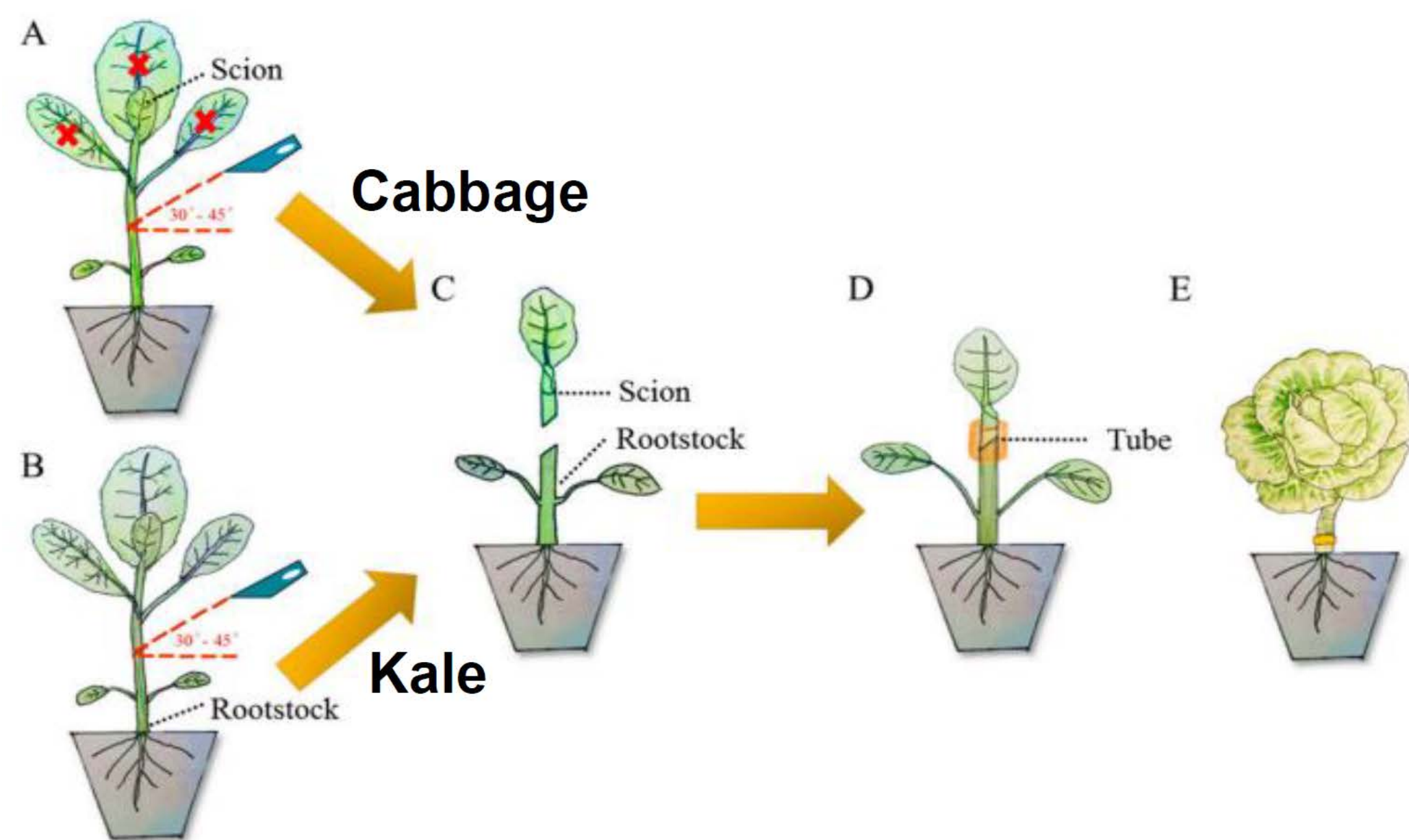
Doping effectiveness among semiconductors

Material	E _g (eV)	μ _e (cm ² /V-s)	μ _h (cm ² /V-s)	V _{sat} (10 ⁷ cm/s)	E _{br} (MV/cm)	σ _{on} (W/cm-K)	N-type	P-type
Ga ₂ O ₃	4.9	180	-	1.1	8	0.11-0.27	Good	Poor
Si	1.12	1350	450	1	0.3	1.5	Good	Good
Ge	0.66	3900	1900	0.6	0.1	0.58	Good	Good
GaAs	1.42	8500	400	1	0.4	0.43	Good	Good
InP	1.34	5400	200	0.67	0.5	0.68	Good	Good

(3) Towards Lattice-Mismatched Heterojunctions:

Semiconductor Grafting

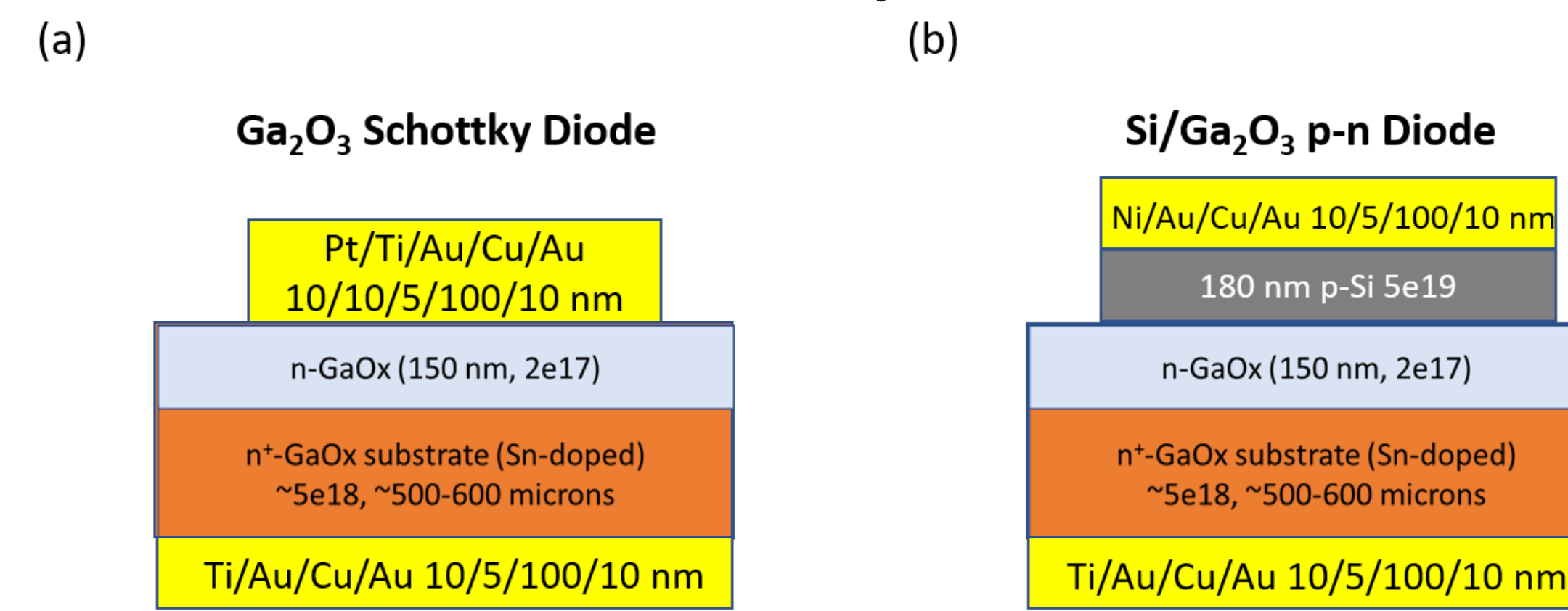
What is GRAFTING technique in nature?



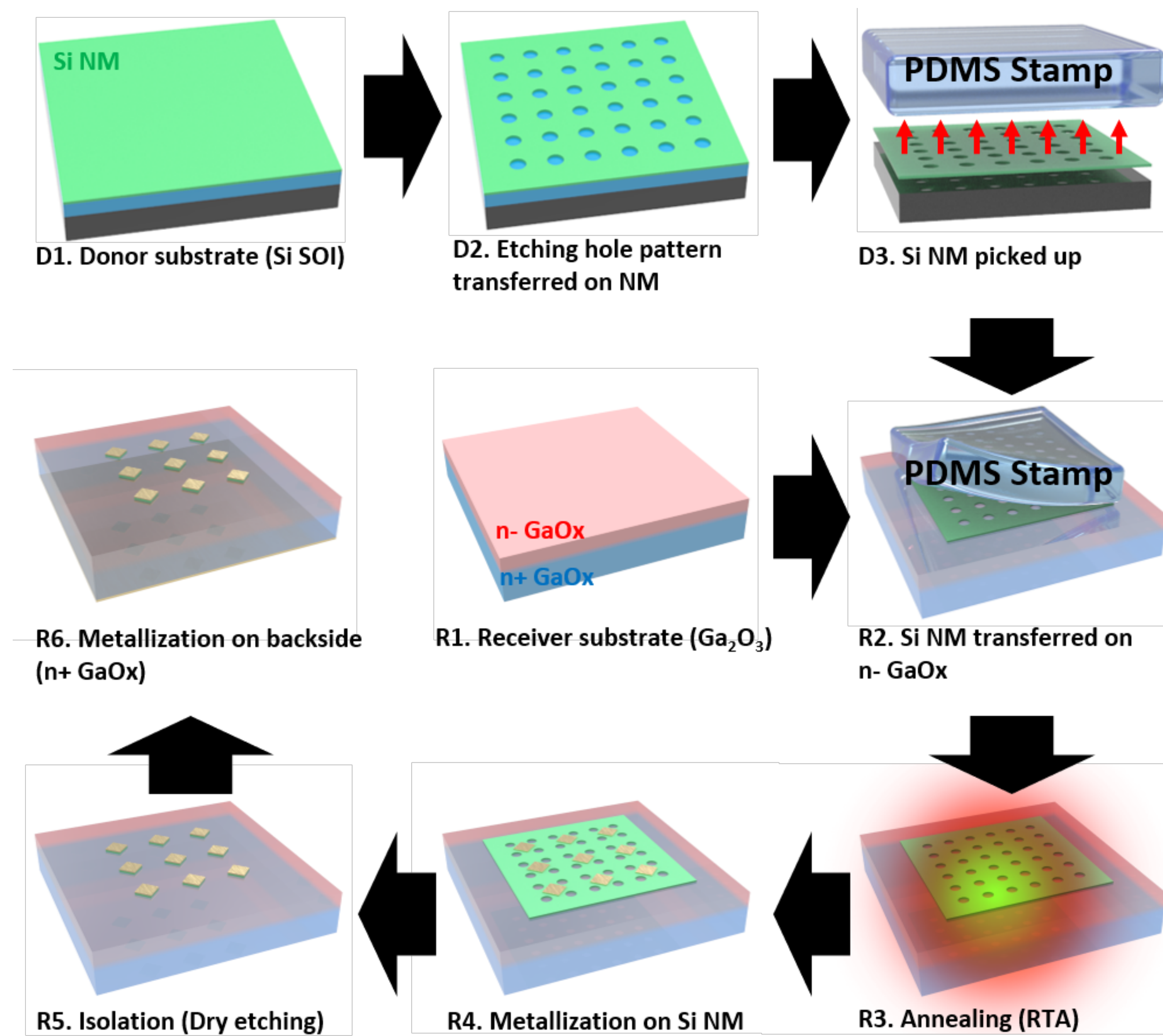
- Semiconductor grafting provided an effective solution to lattice-mismatch encountered by epitaxial growth community.
- **Ultrathin oxide** functions as a passivation and quantum tunneling layer.
- Ultra-low density of interface states (D_{it}): **10¹⁰-10¹¹ /cm².eV**

2. Experiment

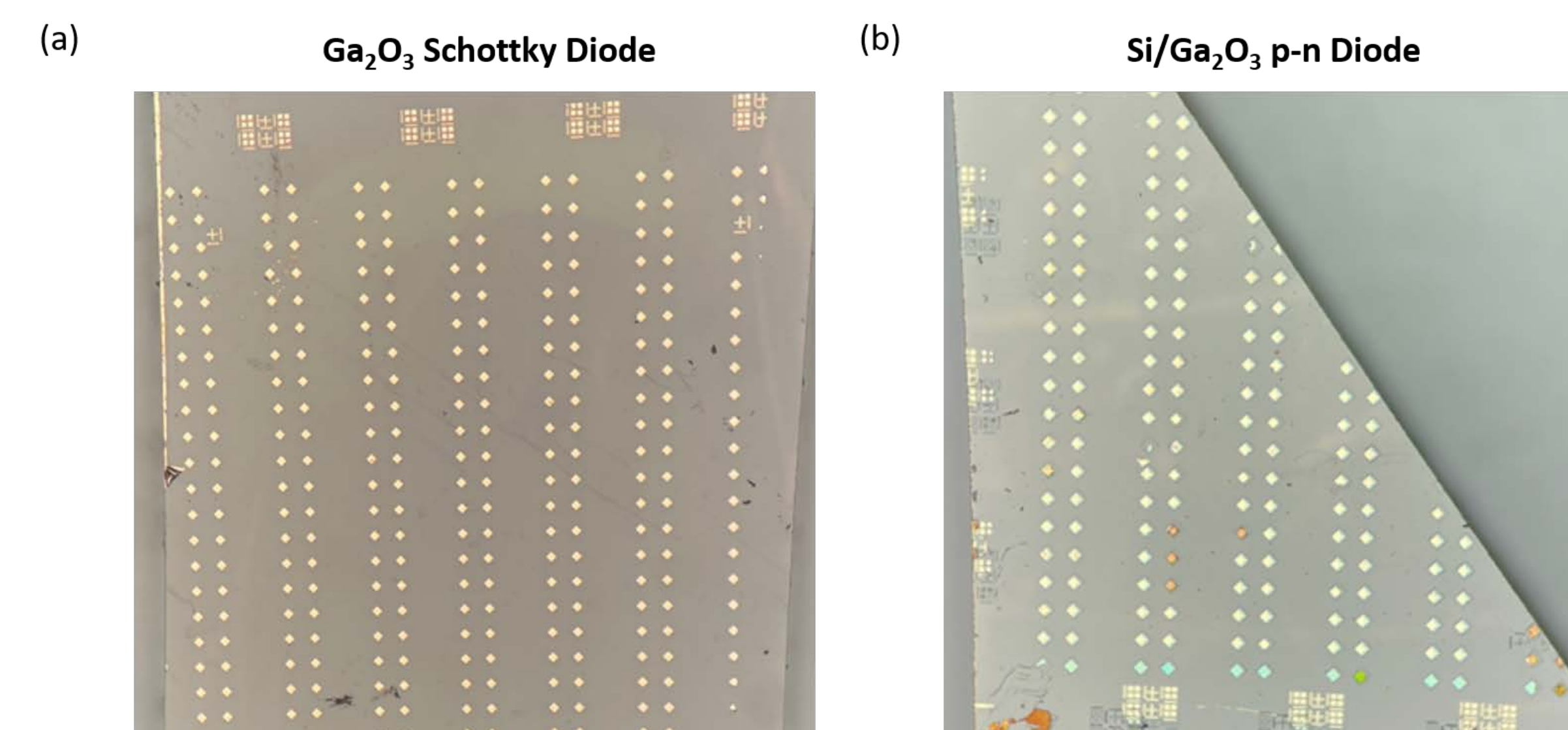
Schematic device layer structure



Schematic fabrication process flow

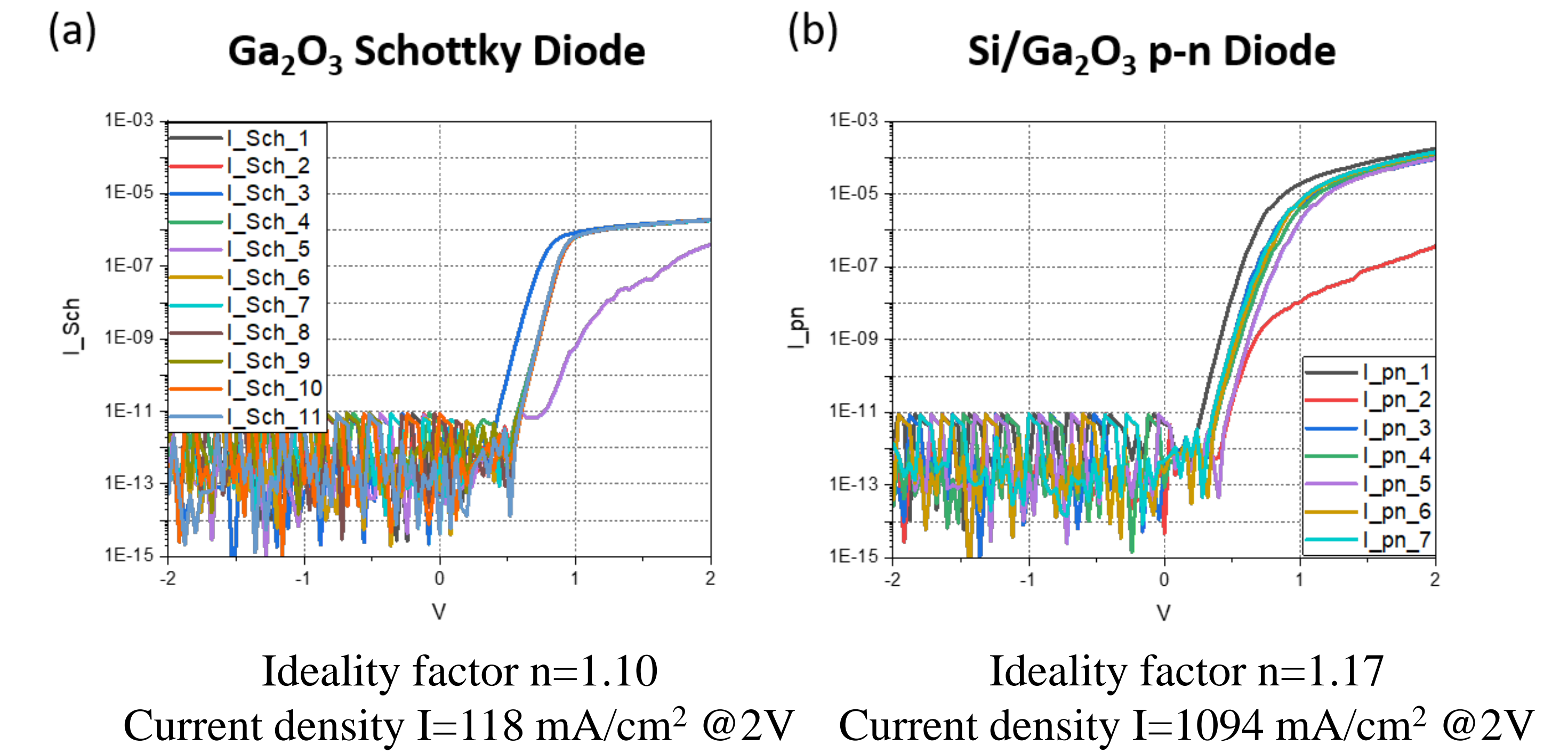


Optical images of the device array

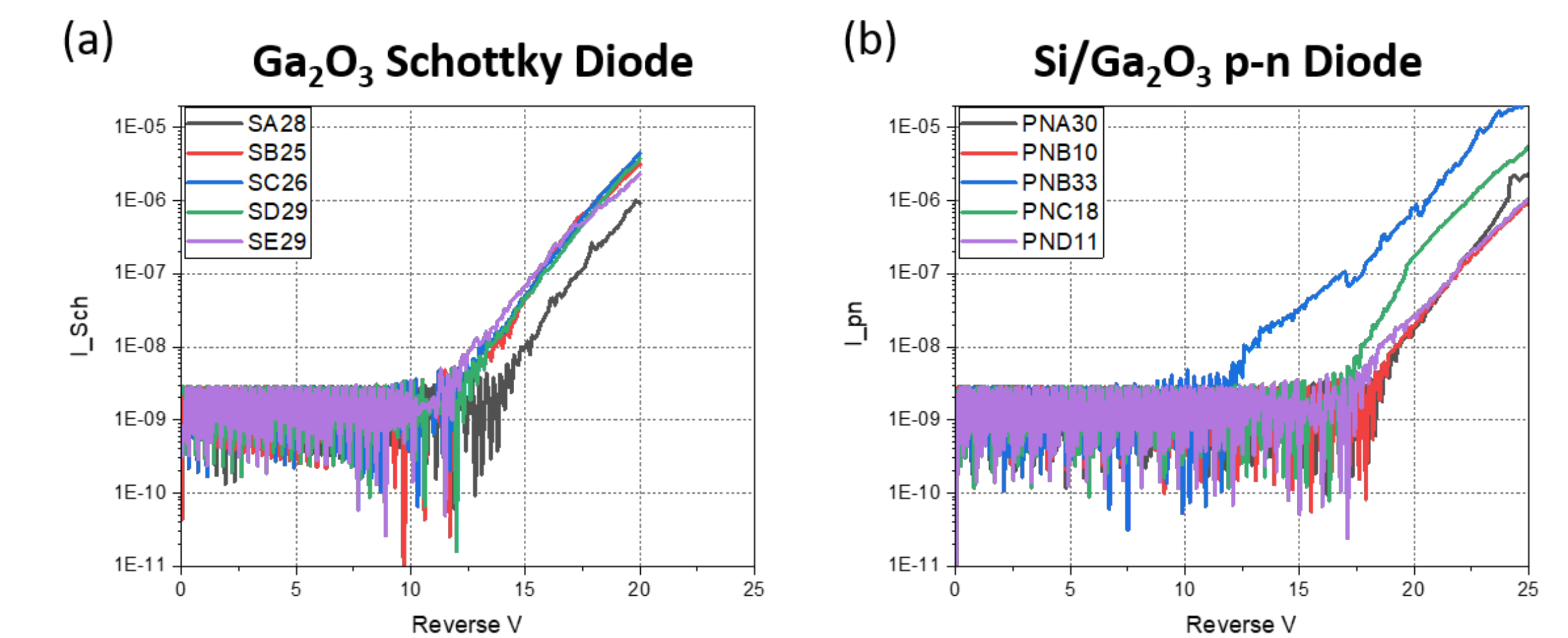


3. Characterizations:

(1) IV measurement



(2) Breakdown measurement



Ga₂O₃ Schottky

Device #	A28	B25	C26	D29	E29
BD (V)	20	18.3	18.1	18.4	18.6

Si/Ga₂O₃ (Annealed)

Device #	A30	B10	B33	C18	D11
BD (V)	24.2	25	20.7	22.4	24.9

4. Conclusions:

- High-quality grafted Si/Ga₂O₃ p-n diodes were fabricated and characterized.
- Higher on/off ratio, good ideality factor, and larger breakdown voltage have been confirmed on the grafted devices than the Schottky diodes.
- Bipolar transistors become feasible.

GOX 2022 Program Overview

Room /Time	Jefferson 1 & Atrium	Jefferson 2-3
MoM		KEY1: Keynote Address AC-MoM: Characterization & Modeling I BG-MoM: Bulk & Epitaxy I
MoA		MD-MoA: Process & Devices I TM-MoA: Characterization & Modelling II
MoP	Poster Sessions: Advanced Characterization Techniques (AC) Dielectric Interfaces (DI) Electronic and Photonic Devices, Circuits and Applications (EP) Electronic Transport & Breakdown Phenomena (ET) Heterogeneous Material Integration (HM)	
TuM		AC-TuM: Advanced Characterization & Microscopy PS1-TuM: Plenary Session I TM-TuM: Characterization & Modelling III
TuA		DI-TuA: Processes & Devices II EG-TuA: Bulk & Epitaxy II
TuP	Poster Sessions: Epitaxial Growth (EG) Material and Device Processing & Fabrication Techniques (MD) Theory, Modeling and Simulation (TM)	
WeM		PS2-WeM: Plenary Session II EP1-WeM: Process & Devices III EP2-WeM: Process and Devices IV

Monday Morning, August 8, 2022

Room Jefferson 2-3		
8:30am	Welcome and Sponsor Thank You	Keynote Address Session KEY1 Keynote Address Moderator: Kelson Chabak , Air Force Research Laboratory
8:45am	INVITED: KEY1-2 Keynote Lecture: Ga ₂ O ₃ Device Technologies: Power Switching and High-Frequency Applications, and Beyond, Masataka Higashiwaki , Department of Physics and Electronics, Osaka Metropolitan University, Japan; T. Kamimura , S. Kumar , Z. Wang , National Institute of Information and Communications Technology, Japan; T. Kitada , J. Liang , N. Shigekawa , Department of Physics and Electronics, Osaka Metropolitan University, Japan; H. Murakami , Y. Kumagai , Department of Applied Chemistry, Tokyo University of Agriculture and Technology, Japan	
9:30am	INVITED: AC-MoM-5 Characterization of Deep Acceptors in β -Ga ₂ O ₃ by Deep Level Optical Spectroscopy, H. Ghadi , J. McGlone , E. Cornuelle , The Ohio State University; A. Senckowski , University of Massachusetts Lowell; S. Sharma , U. Singiseti , University of Buffalo; M. Wong , University of Massachusetts Lowell; A. Arehart , Steven A Ringel , The Ohio State University	Advanced Characterization Techniques Session AC-MoM Characterization & Modeling I Moderator: Kornelius Tetzner , Ferdinand-Braun-Institut, Leibniz-Institut für Höchstfrequenztechnik (FBH), Germany
10:00am	AC-MoM-7 Determination of Cation Vacancy and Al Diffusion Constants in B-(Al,Ga) ₂ O ₃ / Ga ₂ O ₃ Superlattices, H. Yang , A. Levin , B. Eisner , A. Bhattacharyya , P. Ranga , S. Krishnamoorthy , Michael Scarpulla , University of Utah	
10:15am	AC-MoM-8 Defect Characterization in Gallium Oxide and Related Materials Using Terahertz Electron Paramagnetic Resonance Ellipsometry: Fe in Ga ₂ O ₃ , Mathias Schubert , University of Nebraska, Lincoln; S. Richter , Lund University, Sweden; S. Knight , P. Kuehne , Linköping University, Sweden; M. Stokey , R. Korlacki , University of Nebraska-Lincoln; V. Stanishev , Linköping University, Sweden; Z. Galazka , K. Irmischer , Leibniz-Institut fuer Kristallzuechtung, Germany; S. Mu , C. Van de Walle , University of California at Santa Barbara; V. Ivády , MPI Physics of Complex Systems, Germany; O. Bulancea-Lindvall , I. Abrikosov , Linköping University, Sweden; V. Darakchieva , Lund University, Sweden	
10:30am	BREAK	
10:45am	INVITED: BG-MoM-10 β -Ga ₂ O ₃ Growth and Wafer Fabrication, A. Brady , G. Foundos , Chase Scott , Northrop Grumman SYNOPTICS; V. Gambin , Northrop Grumman Corporation; K. Stevens , Northrop Grumman SYNOPTICS; J. Blevins , Air Force Research Laboratory, Afghanistan	Bulk Growth Session BG-MoM Bulk & Epitaxy I Moderator: John Blevins , Air Force Research Laboratory
11:15am	BG-MoM-12 Increasing the Bandgap of β -Ga ₂ O ₃ via Alloying with Al ₂ O ₃ or Sc ₂ O ₃ in Czochralski-grown Crystals, Benjamin Dutton , J. Jesenovec , B. Downing , J. McCloy , Washington State University	
11:30am	BG-MoM-13 Chemi-Mechanical Polishing and Subsurface Damage Characterization of 2-inch (010) Semi-Insulating β -Ga ₂ O ₃ Substrates, David Snyder , Penn State Applied Research Laboratory	
11:45am	BG-MoM-14 Ge-Delta Doped β -Ga ₂ O ₃ Grown Via Plasma Assisted Molecular Beam Epitaxy, Thaddeus Asel , Air Force Research Laboratory, Materials and Manufacturing Directorate, USA; E. Steinbrunner , Wright State University, Department of Electrical Engineering; J. Hendrick , Air Force Institute of Technology, Department of Engineering Physics; A. Neal , S. Mou , Air Force Research Laboratory, Materials and Manufacturing Directorate, USA	
12:00pm	BG-MoM-15 High Purity n-type β -Ga ₂ O ₃ Films with 10 ¹³ cm ⁻³ Residual Acceptor Concentration by MOCVD, Andrei Osinsky , F. Alema , Agnitrion Technology	

Monday Afternoon, August 8, 2022

Room Jefferson 2-3		
1:45pm	INVITED: MD-MoA-1 High Aspect Ratio Ga ₂ O ₃ -based Homo and Heterostructures by Plasma-free Metal-assisted Chemical Etching, <i>Xiuling Li</i> , University of Texas at Austin; <i>H. Huang, C. Chan, J. Michaels</i> , University of Illinois, Urbana-Champaign	Material and Device Processing and Fabrication Techniques Session MD-MoA Process & Devices I Moderator: Man-Hoi Wong , University of Massachusetts Lowell
2:15pm	MD-MoA-3 Blocking Behavior of N and Fe Ion Implanted β -Ga ₂ O ₃ , <i>Bennett Cromer</i> , Cornell University; <i>W. Li</i> , University of California at Berkeley; <i>K. Smith</i> , Cornell University; <i>K. Gann</i> , Cornell University, Iceland; <i>K. Nomoto</i> , Cornell University; <i>N. Hendriks</i> , University of California at Santa Barbara; <i>A. Green, K. Chabak</i> , Air Force Research Laboratory; <i>M. Thompson, D. Jena, G. Xing</i> , Cornell University	
2:30pm	MD-MoA-4 Evolution and Recovery of Ion Implantation-Induced Damage Zone in β -Ga ₂ O ₃ , <i>Elaf Anber, D. Foley, J. Nathaniel</i> , Johns Hopkins University; <i>A. Lang</i> , American Society for Engineering Education; <i>J. Hart</i> , Johns Hopkins University; <i>M. Tadjer, K. Hobart</i> , US Naval Research Laboratory; <i>S. Pearton</i> , University of Florida, Gainesville; <i>M. Taheri</i> , Johns Hopkins University	
2:45pm	MD-MoA-5 Heterogeneous Integration of Single-Crystal β -Ga ₂ O ₃ and N-Polar GaN Substrates With ZnO Interlayer Deposited by Atomic Layer Deposition, <i>Zhe (Ashley) Jian</i> , University of Michigan, Ann Arbor; <i>C. Clymore</i> , University of California, Santa Barbara; <i>D. Agapiou</i> , University of Michigan, Ann Arbor; <i>U. Mishra</i> , University of California, Santa Barbara; <i>E. Ahmadi</i> , University of Michigan, Ann Arbor	
3:00pm	MD-MoA-6 Structural Transformation of β -Ga ₂ O ₃ through Si-implantation, <i>Snorre Braathen Kjeldby, A. Azarov, P. Nguyen</i> , Centre for Materials Science and Nanotechnology, University of Oslo, Norway; <i>V. Venkatachalapathy</i> , Centre for Materials Science and Nanotechnology, University of Oslo and Department of Materials Science, National Research Nuclear University, "MEPhI", Norway; <i>R. Mikšová</i> , Nuclear Physics Institute of the Czech Academy of Sciences, Czechia; <i>A. Macková</i> , Nuclear Physics Institute of the Czech Academy of Sciences and Department of Physics, Faculty of Science, J.E. Purkyně University, Czechia; <i>J. García-Fernández, A. Kuznetsov, Ø. Prytz, L. Vines</i> , Centre for Materials Science and Nanotechnology, University of Oslo, Norway	
3:15pm	MD-MoA-7 Electrical Characteristics of <i>in Situ</i> Mg-Doped Ga ₂ O ₃ Current-Blocking Layer for Vertical Devices, <i>Sudipto Saha</i> , University at Buffalo-SUNY; <i>L. Meng, A. Bhuiyan, Z. Feng, H. Zhao</i> , Ohio State University; <i>U. Singiseti</i> , University at Buffalo-SUNY	
3:30pm	BREAK	
3:45pm	INVITED: TM-MoA-9 Transport, Doping, and Defects in β -Ga ₂ O ₃ , <i>Adam Neal</i> , Air Force Research Laboratory, Materials and Manufacturing Directorate, USA	Theory, Modeling and Simulation Session TM-MoA Characterization & Modelling II Moderator: Mike Thompson , Cornell University
4:15pm	TM-MoA-11 Structural Changes to Beta Gallium Oxide from Ion Irradiation Damage: Model and Relation to in-Situ Experiments, <i>Alexander Petkov, D. Cherns, D. Liu</i> , University of Bristol, UK; <i>W. Chen, M. Li</i> , Argonne National Laboratory, USA; <i>J. Blevins</i> , Air Force Research Laboratory, USA; <i>V. Gambin</i> , Northrop Grumman; <i>M. Kuball</i> , University of Bristol, UK	
4:30pm	TM-MoA-12 Band Structure Across κ -(In _x Ga _{1-x}) ₂ O ₃ / κ -(Al _y Ga _{1-y}) ₂ O ₃ Thin Film Interfaces, <i>Ingvid Julie Thue Jensen, A. Thøgersen, E. Fertitta, B. Belle</i> , SINTEF Materials Physics, Norway; <i>A. Langørgen, S. Cooil, Y. Hommedal, Ø. Prytz, J. Wells, L. Vines</i> , University of Oslo, Norway; <i>H. von Wenckstern</i> , University of Leipzig, Germany	
4:45pm	TM-MoA-13 Aluminum Incorporation Striations in (-201) β -(Al _x Ga _{1-x}) ₂ O ₃ Films Grown on C-Plane and Miscut Sapphire Substrates, <i>Kenny Huynh, Y. Wang, M. Liao</i> , University of California Los Angeles; <i>P. Ranga</i> , University of Utah; <i>S. Krishnamoorthy</i> , University of California at Santa Barbara; <i>M. Goorsky</i> , University of California, Los Angeles	
5:00pm	TM-MoA-14 Plasmon-phonon Coupling in Electrostatically Gated β -Ga ₂ O ₃ Films with Mobility Exceeding 200 cm ² V ⁻¹ s ⁻¹ , <i>A. Rajapitamahuni, A. Manjeshwar</i> , University of Minnesota, USA; <i>A. Kumar, A. Datta</i> , University at Buffalo; <i>P. Ranga</i> , University of California Santa Barbara; <i>L. Thoutam</i> , SR University, Warangal, India; <i>S. Krishnamoorthy</i> , University of California Santa Barbara; <i>Uttam Singiseti</i> , University at Buffalo; <i>B. Jalan</i> , University of Minnesota, USA	

Advanced Characterization Techniques

Room Jefferson 1 & Atrium - Session AC-MoP

Advanced Characterization Techniques Poster Session

5:15pm – 7:15pm

AC-MoP-1 Advanced Defect Characterization in β -Ga₂O₃ Without the Arrhenius Plot, *Jian Li*, NCKU, Taiwan; *A. Neal, S. Mou*, Air Force Research Laboratory, Materials and Manufacturing Directorate, USA; *M. Wong*, University of Massachusetts Lowell

AC-MoP-2 Infrared-Active Phonon Modes and Static Dielectric Constants of Orthorhombic LiGaO₂, *Teresa Gramer, M. Stokey, R. Korlacki, M. Schubert*, University of Nebraska - Lincoln

AC-MoP-3 Spectroscopic Ellipsometry Optical Analysis of Zinc Gallate at Elevated Temperatures, *Emma Williams*, University of Nebraska-Lincoln, USA; *M. Hilfiker, U. Kilic, Y. Traouli, N. Koeppe, J. Rivera, A. Abakar, M. Stokey, R. Korlacki*, University of Nebraska - Lincoln; *Z. Galazka*, Leibniz-Institut für Kristallzüchtung, Germany; *M. Schubert*, University of Nebraska - Lincoln

AC-MoP-4 The Electron Spin Hamiltonian for Fe³⁺ in Monoclinic β -Ga₂O₃, *Steffen Richter*, Lund University, Sweden; *S. Knight, P. Kühne*, Linköping University, Sweden; *M. Schubert*, University of Nebraska - Lincoln; *V. Darakchieva*, Lund University, Sweden

AC-MoP-5 Characterization of (010) β -Ga₂O₃ to Support Fabrication, Wafer Size Scaleup, and Epi Development, *David Snyder*, Penn State Applied Research Laboratory

AC-MoP-6 Photoluminescence Spectroscopy of Cr³⁺ in β -Ga₂O₃ and (Al_{0.1}Ga_{0.9})₂O₃, *Cassandra Remple, J. Jesenovec, B. Dutton, J. McCloy, M. McCluskey*, Washington State University

AC-MoP-7 Surface Relaxation and Rumppling of Sn Doped β -Ga₂O₃(010), *Nick Barrett*, CEA Saclay, France; *A. Pancotti*, Universidade Federal de Jataí, Brazil; *T. Back, AFRL; W. Hamouda, M. Laccheb, C. Lubin, A. Boucly*, CEA Saclay, France; *P. Soukiasian*, Université Paris-Saclay, France; *J. Boeckl, D. Dorsey, S. Mou, T. Asel*, AFRL; *G. Geneste*, CEA, France

AC-MoP-8 Probing Vacancies and Hydrogen Related Defects in β -Ga₂O₃ with Positrons and FTIR, *Corey Halverson, M. Weber, J. Jesenovec, B. Dutton, C. Remple, M. McCluskey, J. McCloy*, Washington State University

AC-MoP-9 Evolution of Anisotropy and Order of Band-to-Band Transitions, Excitons, Phonons, Static and High Frequency Dielectric Constants Including Strain Dependencies in Alpha and Beta Phase (Al_xGa_{1-x})₂O₃, *Megan Stokey*, University of Nebraska-Lincoln; *R. Korlacki, M. Hilfiker, T. Gramer*, University of Nebraska - Lincoln; *J. Knudtson*, University of Nebraska-Lincoln; *S. Richter*, Lund University, Sweden; *S. Knight*, Linköping University, Sweden; *A. Mock*, Weber State University; *A. Mauze, Y. Zhang, J. Speck*, University of California Santa Barbara; *R. Jinno, Y. Cho, H. Xing, D. Jena*, Cornell University; *Y. Oshima*, National Institute for Materials Science, Japan; *E. Ahmadi*, University of Michigan; *V. Darakchieva*, Lund University, Sweden; *M. Schubert*, University of Nebraska - Lincoln

AC-MoP-10 Photoluminescence Mapping of Gallium Oxide and Aluminum Gallium Oxide Epitaxial Films, *Jacqueline Cooke, P. Ranga*, University of Utah; *J. Jesenovec, J. McCloy*, Washington State University; *S. Krishnamoorthy*, University of California at Santa Barbara; *M. Scarpulla, B. Sensale-Rodriguez*, University of Utah

AC-MoP-11 Cathodoluminescence (CL) Evaluation of Silicon Implant Activation and Damage Annealing in Beta Ga₂O₃ EPI in Heavily Silicon Doped Contact Regions, *Stephen Tetlak*, Air Force Research Laboratory; *K. Gann, J. McCandless*, Cornell University; *K. Liddy*, Air Force Research Laboratory; *D. Jenna, M. Thompson*, Cornell University

AC-MoP-12 Non-Destructive Characterization of Annealed Si-Implanted Thin Film β -Ga₂O₃, *Aine Connolly, K. Gann*, Cornell University; *S. Tetlak*, Air Force Research Laboratory; *V. Protasenko*, Cornell University; *M. Slocum, S. Mou*, Air Force Research Laboratory; *M. Thompson*, Cornell University

Dielectric Interfaces

Room Jefferson 1 & Atrium - Session DI-MoP

Dielectric Interfaces Poster Session

5:15pm – 7:15pm

DI-MoP-1 Band Offsets of MOCVD Grown β -(Al_{0.21}Ga_{0.79})₂O₃/ β -Ga₂O₃ (010) Heterojunctions, *T. Morgan, J. Rudie, M. Zamani-Alavijeh, A. Kuchuk*, University of Arkansas; *N. Orishchin, F. Alema*, Agnitron Technology Incorporated; *A. Osinsky*, Agnitron Technology Incorporated, United States Minor Outlying Islands (the); *R. Sleezer*, Minnesota State University at Mankato; *G. Salamo*, University of Arkansas, United States Minor Outlying Islands (the); *Morgan Ware*, University of Arkansas

DI-MoP-2 Optimization of MOCVD Grown In-situ Dielectrics for β -Ga₂O₃, *G. Wang*, University of Wisconsin - Madison; *F. Alema*, Agnitron Technology Inc.; *J. Chen*, University of Wisconsin - Madison; *A. Osinsky*, Agnitron Technology Inc.; *C. Gupta*, University of Wisconsin-Madison; *Shubhra Pasayat*, University of Wisconsin - Madison

Electronic and Photonic Devices, Circuits and Applications

Room Jefferson 1 & Atrium - Session EP-MoP

Electronic and Photonic Devices, Circuits and Applications

Poster Session – 5:15pm – 7:15pm

EP-MoP-1 Investigating Ohmic Contacts for High Temperature Operation of Ga₂O₃ Devices, *William Callahan*, Colorado School of Mines; *S. Sohel*, National Renewable Energy Laboratory; *M. Sanders, R. O'Hayre*, Colorado School of Mines; *D. Ginley, A. Zakutayev*, National Renewable Energy Laboratory

EP-MoP-2 Gate Effects of Channel and Sheet Resistance in β -Ga₂O₃ Field-Effect Transistors using the TLM Method, *Ory Maimon*, Department of Electrical Engineering, George Mason University; *N. Moser*, Air Force Research Laboratory, Sensors Directorate; *K. Liddy, A. Green, K. Chabak*, Air Force Research Laboratory, Sensors Directorate, USA; *C. Richter, K. Cheung, S. Pookpanratana*, Nanoscale Device and Characterization Division, National Institute of Standards and Technology; *Q. Li*, Department of Electrical Engineering, George Mason University

EP-MoP-3 Lateral β -Ga₂O₃ Schottky Barrier Diodes With Interdigitated Contacts, *Jeremiah Williams*, Air Force Research Laboratory, Sensors Directorate; *A. Arias-Purdue, Teledyne; K. Liddy, A. Green*, Air Force Research Laboratory, Sensors Directorate; *D. Dryden, N. Sepelak, KBR; K. Singh*, Air Force Research Laboratory, Sensors Directorate; *F. Alema, A. Osinsky*, Agnitron Technology; *A. Islam, N. Moser, K. Chabak*, Air Force Research Laboratory, Sensors Directorate

EP-MoP-4 Optimized Annealing for Activation of Implanted Si in β -Ga₂O₃, *Katie Gann, J. McCandless*, Cornell University; *T. Asel, S. Tetlak*, Air Force Research Laboratory; *D. Jena, M. Thompson*, Cornell University

Electronic Transport and Breakdown Phenomena

Room Jefferson 1 & Atrium - Session ET-MoP

Electronic Transport and Breakdown Phenomena Poster

Session

5:15pm

ET-MoP-2 Electric Field Mapping in β -Ga₂O₃ by Photocurrent Spectroscopy, *Darpan Verma, M. Adnan, S. Dhara*, Ohio State University; *C. Sturm*, Universität Leipzig, Germany; *S. Rajan, R. Myers*, Ohio State University

ET-MoP-3 Activation of Si, Ge, and Sn Donors in High-Resistivity Halide Vapor Phase Epitaxial β -Ga₂O₃:N, *Joseph Spencer*, Naval Research Laboratory/Virginia Tech CPES; *M. Tadjer, A. Jacobs, M. Mastro, J. Gallagher, J. Freitas, Jr*, Naval Research Laboratory; *T. Tu, A. Kuramata, K. Sasaki*, Novel Crystal, Japan; *Y. Zhang*, Virginia Tech (CPES); *T. Anderson, K. Hobart*, Naval Research Laboratory

Heterogeneous Material Integration

Room Jefferson 1 & Atrium - Session HM-MoP

Heterogeneous Material Integration Poster Session

5:15pm – 7:15pm

HM-MoP-1 Structural and Thermal Transport Analysis of Wafer Bonded β -Ga₂O₃ |4H-SiC, *Michael Liao, K. Huynh, Y. Wang*, UCLA; *Z. Cheng*, UIUC; *J. Shi*, GaTech; *F. Mu*, IMECAS, China; *T. You, W. Xu, X. Ou*, ShanghaiTech, China; *T. Suga*, Meisei University, Japan; *S. Graham*, GaTech; *M. Goorsky*, UCLA

HM-MoP-2 Advances in Plasma-Enhanced Atomic Layer Deposited (PEALD) Ga₂O₃ Films, *Virginia Wheeler, A. Lang, N. Nepal, E. Jin, D. Katzer, V. Gokhale, B. Downey, D. Meyer*, US Naval Research Laboratory

HM-MoP-3 Grafted Si/Ga₂O₃ pn Diodes, *H. Jang, D. Kim*, University of Wisconsin - Madison; *J. Gong*, University of Wisconsin at Madison; *F. Alema, A. Osinsky*, Agnitron Technology Inc.; *K. Chabak*, Air Force Research Laboratory; *G. Jessen*, BAE Systems; *G. Vincent*, Northrup Grumman; *S. Pasayat, C. Gupta*, University of Wisconsin - Madison; *Zhenqiang Ma*, 1415 Engineering Drive

Tuesday Morning, August 9, 2022

Room Jefferson 2-3		
8:30am	Welcome and Sponsor Thank You	Plenary Session Session PS1-TuM Plenary Session I Moderator: Kelson Chabak, Air Force Research Laboratory
8:45am	INVITED: PS1-TuM-2 Plenary Lecture: Gallium Oxide Electronics - Device Engineering Toward Ultimate Material Limits, <i>Siddharth Rajan</i> , The Ohio State University	
9:15am	INVITED: TM-TuM-4 First-Principles Modeling of Ga ₂ O ₃ , <i>Hartwin Peelaers</i> , University of Kansas	Theory, Modeling and Simulation Session TM-TuM Characterization & Modelling III Moderator: Michael Scarpulla, University of Utah
9:45am	TM-TuM-6 Theory of Acceptor-Donor Complexes in Ga ₂ O ₃ , <i>I. Chatratin, F. Sabino</i> , University of Delaware; <i>P. Reunchan</i> , Kasetsart University, Thailand; <i>Anderson Janotti</i> , University of Delaware	
10:00am	TM-TuM-7 Donor Doping of Monoclinic and Corundum (Al _x Ga _{1-x}) ₂ O ₃ , <i>Darshana Wickramaratne</i> , US Naval Research Laboratory; <i>J. Varley</i> , Lawrence Livermore National Laboratory; <i>J. Lyons</i> , US Naval Research Laboratory	
10:15am	TM-TuM-8 The Co-Design, Fabrication, and Characterization of a Ga ₂ O ₃ -on-SiC MOSFET, <i>Yiwen Song</i> , Pennsylvania State University; <i>A. Bhattacharyya</i> , University of Utah; <i>A. Karim, D. Shoemaker</i> , Pennsylvania State University; <i>H. Huang</i> , Ohio State University; <i>C. McGray</i> , Modern Microsystems, Inc.; <i>J. Leach</i> , Kyma Technologies, Inc.; <i>J. Hwang</i> , Ohio State University; <i>S. Krishnamoorthy</i> , University of California at Santa Barbara; <i>S. Choi</i> , Pennsylvania State University	
10:30am	BREAK	
10:45am	INVITED: AC-TuM-10 Defects in Gallium Oxide – How We “See” and Understand Them, <i>Jinwoo Hwang</i> , The Ohio State University	Advanced Characterization Techniques Session AC-TuM Advanced Characterization & Microscopy Moderator: Ginger Wheeler, Naval Research Laboratory
11:15am	AC-TuM-12 Atomic-Scale Investigation of Point and Extended Defects in Ion Implanted β-Ga ₂ O ₃ , <i>Hsien-Lien Huang, C. Chae</i> , The Ohio State University; <i>A. Senckowski, M. Wong</i> , Penn State University; <i>J. Hwang</i> , The Ohio State University	
11:30am	AC-TuM-13 Microscopic and Spectroscopic Analysis of (100), (-201) and (010) (Al _x Ga _{1-x}) ₂ O ₃ Films Using Atom Probe Tomography, <i>J. Sarker</i> , University at Buffalo-SUNY; <i>A. Bhuiyan, Z. Feng, L. Meng, H. Zhao</i> , The Ohio State University; <i>Baishakhi Mazumder</i> , University at Buffalo-SUNY	
11:45am	AC-TuM-14 Phase and Microstructure Evolution of κ-Ga ₂ O ₃ Thin Films Grown by MOCVD, <i>Jingyu Tang, K. Jiang</i> , Carnegie Mellon University, China; <i>M. Cabral, A. Park</i> , Carnegie Mellon University; <i>L. Gu</i> , Carnegie Mellon University, China; <i>R. Davis, L. Porter</i> , Carnegie Mellon University	
12:00pm	AC-TuM-15 Investigation of Extended Defects in Ga ₂ O ₃ Substrates and Epitaxial Layers using X-ray Topography, <i>Nadeemullah A. Mahadik, M. Tadjer, T. Anderson, K. Hobart</i> , Naval Research Laboratory, USA; <i>K. Sasaki, A. Kuramata</i> , Novel Crystal Technology, Japan	

Tuesday Afternoon, August 9, 2022

Room Jefferson 2-3		
1:45pm	INVITED: EG-TuA-1 Progress in Beta-Gallium Oxide Materials and Properties, <i>James Speck</i> , University of California Santa Barbara	Epitaxial Growth Session EG-TuA Bulk & Epitaxy II Moderator: Xiuling Li , University of Texas Austin
2:15pm	EG-TuA-3 (110) β -Ga ₂ O ₃ Epitaxial Films Grown by Plasma-Assisted Molecular Beam Epitaxy, <i>Takeki Itoh</i> , <i>A. Mauze</i> , <i>Y. Zhang</i> , <i>J. Speck</i> , University of California at Santa Barbara	
2:30pm	EG-TuA-4 Si-doped β -Ga ₂ O ₃ Films Grown at 1 μ m/hr by Suboxide MBE, <i>Kathy Azizie</i> , <i>P. Vogt</i> , <i>F. Hensling</i> , <i>D. Schlom</i> , <i>J. McCandless</i> , <i>H. Xing</i> , <i>D. Jena</i> , Cornell University; <i>D. Dryden</i> , <i>A. Neal</i> , <i>S. Mou</i> , <i>T. Asef</i> , <i>A. Islam</i> , <i>A. Green</i> , <i>K. Chabak</i> , Air Force Research Laboratory	
2:45pm	INVITED: EG-TuA-5 MOCVD Growth of Ga ₂ O ₃ and (Al _x Ga _{1-x}) ₂ O ₃ , <i>Hongping Zhao</i> , The Ohio State University	
3:15pm		
3:30pm	BREAK	
3:45pm	DI-TuA-9 Dielectric Integration on (010) β -Ga ₂ O ₃ : Al ₂ O ₃ , SiO ₂ Interfaces and their Thermal Stability, <i>Ahmad Islam</i> , Air Force Research Laboratory; <i>A. Miesle</i> , University of Dayton; <i>M. Dietz</i> , Wright State University; <i>K. Leedy</i> , <i>S. Ganguli</i> , Air Force Research Laboratory; <i>G. Subramanyam</i> , University of Dayton; <i>W. Wang</i> , Wright State University; <i>N. Sepelak</i> , <i>D. Dryden</i> , KBR, Inc.; <i>T. Asef</i> , <i>A. Neal</i> , <i>S. Mou</i> , <i>S. Tetlak</i> , <i>K. Liddy</i> , <i>A. Green</i> , <i>K. Chabak</i> , Air Force Research Laboratory	Dielectric Interfaces Session DI-TuA Processes & Devices II Moderator: Hongping Zhao , Ohio State University
4:00pm	DI-TuA-10 Deep Etch Field-Terminated β -Ga ₂ O ₃ Schottky Barrier Diodes With 4.2 MV/cm Parallel Plate Field Strength, <i>Sushovan Dhara</i> , <i>N. Kalarickala</i> , <i>A. Dheenana</i> , <i>C. Joishi</i> , <i>S. Rajan</i> , The Ohio State University	
4:15pm	DI-TuA-11 Demonstration of Low Thermal Resistance in Ga ₂ O ₃ Schottky Diodes by Junction-Side-Cooled Packaging, <i>Boyan Wang</i> , <i>M. Xiao</i> , <i>J. Knoll</i> , <i>Y. Qin</i> , Virginia Polytechnic Institute and State University; <i>J. Spencer</i> , U.S. Naval Research Laboratory; <i>M. Tadjer</i> , U.S. Naval Research Laboratory; <i>C. Buttay</i> , Univ Lyon, CNRS, INSA Lyon, Université Claude Bernard Lyon 1, Ecole Centrale de Lyon, Ampère, France; <i>K. Sasaki</i> , Novel Crystal Technology, Japan; <i>G. Lu</i> , <i>C. DiMarino</i> , <i>Y. Zhang</i> , Virginia Polytechnic Institute and State University	
4:30pm	DI-TuA-12 High Temperature In-situ MOCVD-grown Al ₂ O ₃ Dielectric on (010) β -Ga ₂ O ₃ with 10 MV/cm Breakdown Field, <i>Saurav Roy</i> , University of California Santa Barbara; <i>A. Bhattacharyya</i> , University of Utah; <i>C. Peterson</i> , <i>S. Krishnamoorthy</i> , University of California Santa Barbara	
4:45pm	DI-TuA-13 Metal Oxide (PtOX) Schottky Contact with High-k Dielectric Field Plate for Improved Field Management in Vertical β -Ga ₂ O ₃ Devices, <i>Esmat Farzana</i> , University of California Santa Barbara; <i>A. Bhattacharyya</i> , The University of Utah; <i>T. Itoh</i> , <i>S. Krishnamoorthy</i> , <i>J. Speck</i> , University of California Santa Barbara	
5:00pm	DI-TuA-14 Field Plated β -Ga ₂ O ₃ Mis Diodes with High-k TiO ₂ Interlayer for Increased Breakdown and Reduced Leakage Current, <i>Nolan Hendricks</i> , Air Force Research Laboratory; UC Santa Barbara; <i>A. Green</i> , <i>A. Islam</i> , <i>K. Leedy</i> , <i>K. Liddy</i> , <i>J. Williams</i> , Air Force Research Lab; <i>E. Farzana</i> , <i>J. Speck</i> , UC Santa Barbara; <i>K. Chabak</i> , Air Force Research Lab	

Epitaxial Growth

Room Jefferson 1 & Atrium - Session EG-TuP

Epitaxial Growth Poster Session

5:15pm – 7:15pm

EG-TuP-1 α -phase Gallium Oxide Thin Films Stabilized on a-, r- and m-plane Sapphire Substrates via Reactive Magnetron Sputtering and Pulsed Laser Deposition, *Edgars Butanovs*, Institute of Solid State Physics University of Latvia

EG-TuP-2 Epitaxial Growth of $(Al_xGa_{1-x})_2O_3$ by Suboxide MBE, *Jacob Steele, K. Azizie, J. McCandless*, Cornell University; *T. Asef*, Air Force Research Lab; *H. Xing, D. Jena, D. Schlom*, Cornell University

EG-TuP-3 LPCVD Grown n- Ga_2O_3 on p-GaN and Demonstration of p-n Heterojunction Behavior, *Arnab Mondal, A. Nandi, M. Yadav*, Indian Institute of Technology Mandi, India; *A. Bag*, Indian Institute of Technology Guwahati, India

EG-TuP-5 Free Carrier Control in Homoepitaxial β - Ga_2O_3 Thin Films by Tin Impurity Doping, *Neeraj Nepal, B. Downey, V. Wheeler, D. Katzer, E. Jin, M. Hardy, V. Gokhale, T. Growden*, US Naval Research Laboratory; *K. Chabak*, Air Force Research Laboratory; *D. Meyer*, US Naval Research Laboratory

EG-TuP-6 MBE Growth of Doped and Insulating Homoepitaxial β - Ga_2O_3 , *Jon McCandless, V. Protasenko, B. Morell*, Cornell University; *E. Steinbrunner, A. Neal*, Air Force Research Laboratory, Materials and Manufacturing Directorate, USA; *Y. Cho, N. Tanen, H. Xing, D. Jena*, Cornell University

EG-TuP-7 High Conductivity Homoepitaxial β - Ga_2O_3 Regrowth Layers by Pulsed Laser Deposition, *Hyung Min Jeon*, KBR; *K. Leedy*, Air Force Research Laboratory

EG-TuP-8 Low-Temperature Epitaxial Growth and in Situ Atomic Layer Doping of β - Ga_2O_3 Films via Plasma-Enhanced ALD. *Saidjafarzoda Ilhom, A. Mohammad, J. Grasso, B. Willis*, University of Connecticut; *A. Okyay*, Stanford University; *N. Biyikli*, University of Connecticut

EG-TuP-9 Highly conductive β - Ga_2O_3 and $(Al_xGa_{1-x})_2O_3$ epitaxial films by MOCVD, *Fikadu Alema*, Agnitron Technology; *T. Itoh, J. Speck*, Materials Department, University of California, Santa Barbara; *A. Osinsky*, Agnitron Technology

Material and Device Processing and Fabrication Techniques

Room Jefferson 1 & Atrium - Session MD-TuP

Material and Device Processing and Fabrication Techniques

Poster Session – 5:00pm – 7:00pm

MD-TuP-1 Record Low Specific Resistance Ohmic Contacts to Highly Doped MOVPE-Grown β - Ga_2O_3 and β - $(Al_xGa_{1-x})_2O_3$ Epitaxial Films, *Carl Peterson*, University of California Santa Barbara; *F. Alema*, Agnitron Technology; *S. Roy*, University of California Santa Barbara; *A. Bhattacharyya*, University of Utah; *A. Osinsky*, Agnitron Technology; *S. Krishnamoorthy*, University of California Santa Barbara

MD-TuP-3 MOCVD β - Ga_2O_3 Gate-recessed MEFET, *Hannah Masten, J. Lundh, J. Spencer*, US Naval Research Laboratory; *F. Alema, A. Osinsky*, Agnitron Technology; *A. Jacobs, K. Hobart, M. Tadjer*, US Naval Research Laboratory

MD-TuP-4 Subsurface Damage Analysis of Chemical Mechanical Polished (010) β - Ga_2O_3 Substrates, *Michael Liao, K. Huynh, L. Matto, D. Lucciani, M. Goorsky*, UCLA

MD-TuP-5 Diffusion of Zn in β - Ga_2O_3 , *Ylva Knausgård Hommedal, Y. Frodason, L. Vines, K. Johansen*, Centre for Materials Science and Nanotechnology/Dep. of Physics, University of Oslo, Norway

MD-TuP-6 Initial Nucleation of Metastable γ - Ga_2O_3 During sub-Millisecond Thermal Anneals of Amorphous Ga_2O_3 , *Katie Gann, C. Chang, M. Chang, D. Sutherland, A. Connolly, D. Muller, R. van Dover, M. Thompson*, Cornell University

MD-TuP-7 Heavily Doped β - Ga_2O_3 Deposited by Magnetron Sputtering, *Adetayo Adedeji*, Elizabeth City State University; *J. Lawson, C. Ebbing*, University of Dayton Research Institute; *J. Merrett*, Air Force Research Laboratory

MD-TuP-8 Point Defect Distributions in Ultrafast Laser Induced Periodic Surface Structures on β - Ga_2O_3 , *D. Ramdin, E. DeAngelis, M. Noor, M. Haseman, E. Chowdhury, Leonard Brillson*, Ohio State University

Theory, Modeling and Simulation

Room Jefferson 1 & Atrium - Session TM-TuP

Theory, Modeling and Simulation Poster Session

5:00pm - 7:00pm

TM-TuP-1 Simulation Study of Single Event Effects in Ga_2O_3 Schottky Diodes, *Animesh Datta, U. Singiseti*, University at Buffalo

TM-TuP-2 Anisotropic Photoresponsivity and Deviation from Beer-Lambert Law in Beta Gallium Oxide, *Md Mahsinur Rahman Adnan, D. Verma, S. Dhara*, The Ohio State University; *C. Sturm*, Universitat Leipzig, Germany; *S. Rajan, R. Myers*, The Ohio State University

TM-TuP-4 Self-Trapped Holes and Polaronic Acceptors in Ultrawide Bandgap Oxides, *John Lyons*, US Naval Research Laboratory

TM-TuP-5 Modeling for a High-Temperature Ultra-Wide Bandgap Gallium Oxide Power Module, *Benjamin Albano*, Virginia Tech Center for Power Electronics Systems; *B. Wang, C. DiMarino, Y. Zhang*, Virginia Tech Center for Power Electronics

TM-TuP-6 Atomic Surface Structure of Sn doped β - $Ga_2O_3(010)$ Studied by Low-energy Electron Diffraction, *Alexandre Pancotti*, Universidade Federal de Jatai, Brazil; *J. T. Sadowski*, Center for Functional Nanomaterials, Brookhaven National Laboratory; *A. Sandre Kilian*, Universidade Federal de Jatai, Brazil; *D. Duarte dos Reis*, Universidade Federal do Mato Grosso do Sul, Brazil; *C. Lubin*, SPEC, CEA, CNRS, Université Paris-Saclay, CEA Saclay, France; *A. Boucly*, SPEC, CEA, CNRS, Université Paris-Saclay, France; *P. Soukiasian*, SPEC, CEA, CNRS, Université Paris-Saclay, CEA Saclay, France; *J. Boeckl, D. Dorsey*, Air Force Research Laboratory; *M. Shin, T. ASEL*, Air Force Research Lab; *J. Brown, N. Barrett*, SPEC, CEA, CNRS, Université Paris-Saclay, CEA Saclay, France; *T. Back*, SPEC, CEA, CNRS, Université Paris-Saclay, CEA Saclay

Wednesday Morning, August 10, 2022

Room Jefferson 2-3		
8:30am	Welcome and Sponsor Thank You	Plenary Session Session PS2-WeM Plenary Session II Moderator: Kelson Chabak , Air Force Research Laboratory
8:45am	INVITED: PS2-WeM-2 Plenary Lecture: Fundamental Limits of Ga ₂ O ₃ Power Devices and How to Get There, Huili Grace Xing , Cornell University	
9:15am	EP-WeM-4 Remarkable Improvement of Conductivity in B-Ga ₂ O ₃ by High-Temperature Si Ion Implantation, Arka Sardar , T. Isaacs-Smith , S. Dhar , Auburn University; J. Lawson , N. Merrett , Air Force Research Laboratory, USA	Electronic and Photonic Devices, Circuits and Applications Session EP-WeM Process & Devices III Moderator: Uttam Singiseti , University of Buffalo, SUNY
9:30am	INVITED: EP-WeM-5 Towards Lateral and Vertical Ga ₂ O ₃ Transistors for High Voltage Power Switching, Kornelius Tetzner , J. Würfl , E. Bahat-Treidel , O. Hilt , Ferdinand-Braun-Institut, Leibniz-Institut für Höchstfrequenztechnik (FBH), Germany; Z. Galazka , S. Bin Anooz , A. Popp , Leibniz-Institut für Kristallzüchtung (IKZ), Germany	
10:00am	EP-WeM-7 Comparison of β -Ga ₂ O ₃ Mosfets With TiW and NiAu Metal Gates for High-Temperature Operation, Nicholas Sepelak , KBR, Wright State University; D. Dryden , KBR; R. Kahler , University of Texas at Dallas; J. William , Air Force Research Lab, Sensors Directorate; T. Asef , Air Force Research Laboratory, Materials and Manufacturing Directorate; H. Lee , University of Illinois at Urbana-Champaign; K. Gann , Cornell University; A. Popp , Leibniz-Institut für Kristallzüchtung, Germany; K. Liddy , Air Force Research Lab, Sensors Directorate; K. Leedy , Air Force Research Laboratory, Sensors Directorate; W. Wang , Wright State University; W. Zhu , University of Illinois at Urbana-Champaign; M. Thompson , Cornell University; S. Mou , Air Force Research Laboratory, Materials and Manufacturing Directorate, USA; K. Chabak , A. Green , Air Force Research Laboratory, Sensors Directorate; A. Islam , Air Force Research Laboratory, Sensors Directorate	
10:15am	EP-WeM-8 High Electron Mobility Si-doped β -Ga ₂ O ₃ MESFETs, Arkka Bhattacharyya , University of Utah; S. Roy , University of California at Santa Barbara; P. Ranga , University of Utah; S. Krishnamoorthy , University of California at Santa Barbara	
10:30am	BREAK	
10:45am	EP2-WeM-10 β -Ga ₂ O ₃ Lateral FinFETs Formed by Atomic Ga Flux Etching, Ashok Dheenan , N. Kalarickal , Z. Feng , L. Meng , The Ohio State University; A. Fiedler , IKZ Berlin, Germany; C. Joishi , A. Price , J. McGlone , S. Dhara , S. Ringel , H. Zhao , S. Rajan , The Ohio State University	Electronic and Photonic Devices, Circuits and Applications Session EP2-WeM Process and Devices IV Moderator: Christina DiMarino , Virginia Tech
11:00am	EP2-WeM-11 Insights Into the Behaviour of Leakage Current in Lateral Ga ₂ O ₃ Transistors on Semi-Insulating Substrates, Zequan Chen , A. Mishra , M. Smith , T. Moule , University of Bristol, UK; M. Uren , University of Bristol, UK; S. Kumar , M. Higashiwaki , National Institute of Information and Communications Technology, Japan; M. Kuball , University of Bristol, UK	
11:15am	EP2-WeM-12 Device Figure of Merit Performance of Scaled Gamma-Gate β -Ga ₂ O ₃ MOSFETs, Kyle Liddy , A. Islam , J. Williams , D. Walker , N. Moser , D. Dryden , N. Sepelak , K. Chabak , A. Green , AFRL	
11:30am	EP2-WeM-13 Electromigration of Native Point Defects and Breakdown in Ga ₂ O ₃ Vertical Devices, M. Haseaman , D. Ramdin , Ohio State University; W. Li , K. Nomoto , D. Jena , G. Xing , Cornell University; Leonard Brillson , Ohio State University	
11:45am	Closing Remarks, Sponsor Thank You, & Collection of e-Surveys	

Author Index

Bold page numbers indicate presenter

— A —

Abakar, A.: AC-MoP-3, 4
Abrikosov, I.: AC-MoM-8, 2
Adedeji, A.: MD-TuP-7, **8**
Adnan, M.: ET-MoP-2, 4; TM-TuP-2, **8**
Agapiou, D.: MD-MoA-5, 3
Ahmadi, E.: AC-MoP-9, 4; MD-MoA-5, 3
Albano, B.: TM-TuP-5, **8**
Albrecht, M.: EG-TuA-7, 7
Alema, F.: BG-MoM-15, 2; DI-MoP-1, 4;
DI-MoP-2, 4; EG-TuP-9, **8**; EP-MoP-3, 4;
HM-MoP-3, 4; MD-TuP-1, 8; MD-TuP-3,
8
Anber, E.: MD-MoA-4, **3**
Anderson, T.: AC-TuM-15, 6; ET-MoP-3,
4
Arehart, A.: AC-MoM-5, 2
Arias-Purdue, A.: EP-MoP-3, 4
Asel, T.: AC-MoP-7, 4; BG-MoM-14, **2**;
DI-TuA-9, 7; EG-TuA-4, 7; EG-TuP-2, 8;
EP-MoP-4, 4; EP-WeM-7, 9
ASEL, T.: TM-TuP-6, 8
Azarov, A.: MD-MoA-6, 3
Azizie, K.: EG-TuA-4, **7**; EG-TuP-2, 8

— B —

Back, T.: AC-MoP-7, 4; TM-TuP-6, 8
Bag, A.: EG-TuP-3, 8
Bahat-Treidel, E.: EP-WeM-5, 9
Barrett, N.: TM-TuP-6, 8
Barrett, N.: AC-MoP-7, **4**
Bassim, N.: HM-MoP-4, 5
Belle, B.: TM-MoA-12, 3
Bhattacharyya, A.: DI-TuA-12, 7
Bhattacharyya, A.: AC-MoM-7, 2; TM-
TuM-8, 6
Bhattacharyya, A.: DI-TuA-13, 7
Bhattacharyya, A.: MD-TuP-1, 8
Bhattacharyya, A.: EP-WeM-8, **9**
Bhuiyan, A.: AC-TuM-13, 6; MD-MoA-7,
3
Bin Anooz, S.: EG-TuA-7, 7; EP-WeM-5, 9
Biyikli, N.: EG-TuP-8, 8
Blevins, J.: BG-MoM-10, 2; TM-MoA-11,
3
Boeckl, J.: AC-MoP-7, 4; TM-TuP-6, 8
Boucly, A.: AC-MoP-7, 4; TM-TuP-6, 8
Brady, A.: BG-MoM-10, 2
Brillson, L.: EP2-WeM-13, **9**; MD-TuP-8,
8
Brown, J.: TM-TuP-6, 8
Bulancea-Lindvall, O.: AC-MoM-8, 2
Butanovs, E.: EG-TuP-1, **8**
Buttay, C.: DI-TuA-11, 7

— C —

Cabral, M.: AC-TuM-14, 6
Callahan, W.: EP-MoP-1, **4**
Chabak, K.: DI-TuA-14, 7; DI-TuA-9, 7;
EG-TuA-4, 7; EG-TuP-5, 8; EP2-WeM-12,
9; EP-MoP-2, 4; EP-MoP-3, 4; EP-WeM-
7, 9; HM-MoP-3, 4; MD-MoA-3, 3
Chae, C.: AC-TuM-12, 6
Chan, C.: MD-MoA-1, 3

Chang, C.: MD-TuP-6, 8
Chang, M.: MD-TuP-6, 8
Chatratin, I.: TM-TuM-6, 6
Chen, J.: DI-MoP-2, 4
Chen, W.: TM-MoA-11, 3
Chen, Z.: EP2-WeM-11, **9**
Cheng, Z.: HM-MoP-1, 4
Cherns, D.: TM-MoA-11, 3
Cheung, K.: EP-MoP-2, 4
Cho, Y.: AC-MoP-9, 4; EG-TuP-6, 8
Choi, S.: TM-TuM-8, 6
Choi, T.: ET-MoP-1, **4**
Chou, T.: EG-TuA-7, 7
Chowdhury, E.: MD-TuP-8, 8
Clymore, C.: MD-MoA-5, 3
Connolly, A.: AC-MoP-12, **4**; MD-TuP-6,
8
Cooil, S.: TM-MoA-12, 3
Cooke, J.: AC-MoP-10, **4**
Cornuelle, E.: AC-MoM-5, 2
Cromer, B.: MD-MoA-3, **3**

— D —

Darakchieva, V.: AC-MoM-8, 2; AC-MoP-
4, 4; AC-MoP-9, 4; TM-TuP-3, 8
Datta, A.: TM-MoA-14, 3; TM-TuP-1, **8**
Davis, R.: AC-TuM-14, 6
DeAngelis, E.: MD-TuP-8, 8
Dhar, S.: EP-WeM-4, 9
Dhara, S.: DI-TuA-10, **7**; EP2-WeM-10, 9;
ET-MoP-2, 4; TM-TuP-2, 8
Dheenana, A.: DI-TuA-10, 7; EP2-WeM-
10, **9**
Dietz, M.: DI-TuA-9, 7
DiMarino, C.: DI-TuA-11, 7; TM-TuP-5, 8
Dong, C.: HM-MoP-4, 5
Dorsey, D.: TM-TuP-6, 8
Dorsey, D.: AC-MoP-7, 4
Downey, B.: EG-TuP-5, 8; HM-MoP-2, 4
Downing, B.: BG-MoM-12, 2
Dryden, D.: DI-TuA-9, 7; EG-TuA-4, 7;
EP2-WeM-12, 9; EP-MoP-3, 4; EP-WeM-
7, 9
Duarte dos Reis, D.: TM-TuP-6, 8
Dutton, B.: AC-MoP-6, 4; AC-MoP-8, 4;
BG-MoM-12, **2**

— E —

Ebbing, C.: MD-TuP-7, 8
Eisner, B.: AC-MoM-7, 2
El-Sherif, H.: HM-MoP-4, 5

— F —

Farzana, E.: DI-TuA-13, **7**; DI-TuA-14, 7
Feng, Z.: AC-TuM-13, 6; EP2-WeM-10, 9;
MD-MoA-7, 3
Fertitta, E.: TM-MoA-12, 3
Fiedler, A.: EP2-WeM-10, 9
Foley, D.: MD-MoA-4, 3
Foundos, G.: BG-MoM-10, 2
Freitas, Jr, J.: ET-MoP-3, 4
Frodason, Y.: MD-TuP-5, 8

— G —

Galazka, Z.: AC-MoM-8, 2; AC-MoP-3, 4;
EG-TuA-7, 7; EP-WeM-5, 9
Gallagher, J.: ET-MoP-3, 4
Gambin, V.: BG-MoM-10, 2; TM-MoA-
11, 3
Ganguli, S.: DI-TuA-9, 7
Gann, K.: AC-MoP-11, 4; AC-MoP-12, 4;
EP-MoP-4, **4**; EP-WeM-7, 9; MD-MoA-3,
3; MD-TuP-6, **8**
García-Fernández, J.: MD-MoA-6, 3
Geneste, G.: AC-MoP-7, 4
Ghadi, H.: AC-MoM-5, 2
Ginley, D.: EP-MoP-1, 4
Gokhale, V.: EG-TuP-5, 8; HM-MoP-2, 4
Gong, J.: HM-MoP-3, 4
Goorsky, M.: HM-MoP-1, 4; MD-TuP-4,
8; TM-MoA-13, 3
Graham, S.: HM-MoP-1, 4
Gramer, T.: AC-MoP-2, **4**; AC-MoP-9, 4
Grasso, J.: EG-TuP-8, 8
Green, A.: DI-TuA-14, 7; DI-TuA-9, 7; EG-
TuA-4, 7; EP2-WeM-12, 9; EP-MoP-2, 4;
EP-MoP-3, 4; EP-WeM-7, 9; MD-MoA-3,
3
Growden, T.: EG-TuP-5, 8
Grüneberg, R.: EG-TuA-7, 7
Gu, L.: AC-TuM-14, 6
Gupta, C.: DI-MoP-2, 4; HM-MoP-3, 4

— H —

Halverson, C.: AC-MoP-8, **4**
Hamouda, W.: AC-MoP-7, 4
Hardy, M.: EG-TuP-5, 8
Hart, J.: MD-MoA-4, 3
Haseman, M.: EP2-WeM-13, 9; MD-TuP-
8, 8
Hendrick, J.: BG-MoM-14, 2
Hendricks, N.: DI-TuA-14, **7**
Hendriks, N.: MD-MoA-3, 3
Hensling, F.: EG-TuA-4, 7
Higashiwaki, M.: EP2-WeM-11, 9; KEY1-
2, **2**
Hilfiker, M.: AC-MoP-3, 4; AC-MoP-9, 4;
TM-TuP-3, 8
Hilt, O.: EP-WeM-5, 9
Hobart, K.: AC-TuM-15, 6; ET-MoP-3, 4;
MD-MoA-4, 3; MD-TuP-3, 8
Holoviak, S.: HM-MoP-4, 5
Hommedal, Y.: MD-TuP-5, **8**; TM-MoA-
12, 3
Huang, H.: AC-TuM-12, 6; MD-MoA-1, 3;
TM-TuM-8, 6
Huynh, K.: HM-MoP-1, 4; MD-TuP-4, 8;
TM-MoA-13, **3**
Hwang, J.: AC-TuM-10, **6**; AC-TuM-12, 6;
TM-TuM-8, 6

— I —

Ilhom, S.: EG-TuP-8, **8**
Irmischer, K.: AC-MoM-8, 2; EG-TuA-7, 7
Isaacs-Smith, T.: EP-WeM-4, 9

Author Index

Islam, A.: DI-TuA-14, 7; DI-TuA-9, **7**; EG-TuA-4, 7; EP2-WeM-12, 9; EP-MoP-3, 4; EP-WeM-7, 9
Itoh, T.: EG-TuP-9, 8
Itoh, T.: DI-TuA-13, 7; EG-TuA-3, 7
Ivády, V.: AC-MoM-8, 2

— J —

Jacobs, A.: ET-MoP-3, 4; MD-TuP-3, 8
Jalan, B.: TM-MoA-14, 3
Jang, H.: HM-MoP-3, 4
Janotti, A.: TM-TuM-6, **6**
Jena, D.: AC-MoP-9, 4; EG-TuA-4, 7; EG-TuP-2, 8; EG-TuP-6, 8; EP2-WeM-13, 9; EP-MoP-4, 4; MD-MoA-3, 3
Jenna, D.: AC-MoP-11, 4
Jensen, I.: TM-MoA-12, **3**
Jeon, H.: EG-TuP-7, **8**
Jesenovec, J.: AC-MoP-10, 4; AC-MoP-6, 4; AC-MoP-8, 4; BG-MoM-12, 2
Jessen, G.: HM-MoP-3, 4
Jian, Z.: MD-MoA-5, **3**
Jiang, K.: AC-TuM-14, 6
Jin, E.: EG-TuP-5, 8; HM-MoP-2, 4
Jinno, R.: AC-MoP-9, 4
Johansen, K.: MD-TuP-5, 8
Joishi, C.: DI-TuA-10, 7; EP2-WeM-10, 9

— K —

Kahler, R.: EP-WeM-7, 9
Kalarickal, N.: EP2-WeM-10, 9
Kalarickala, N.: DI-TuA-10, 7
Kamimura, T.: KEY1-2, 2
Karim, A.: TM-TuM-8, 6
Katzer, D.: EG-TuP-5, 8; HM-MoP-2, 4
Kilic, U.: AC-MoP-3, 4
Kim, D.: HM-MoP-3, 4
Kitada, T.: KEY1-2, 2
Kjeldby, S.: MD-MoA-6, **3**
Knight, S.: AC-MoM-8, 2; AC-MoP-4, 4; AC-MoP-9, 4
Knoll, J.: DI-TuA-11, 7
Knudtson, J.: AC-MoP-9, 4; TM-TuP-3, 8
Koeppel, N.: AC-MoP-3, 4
Korlacki, R.: AC-MoM-8, 2; AC-MoP-2, 4; AC-MoP-3, 4; AC-MoP-9, 4; TM-TuP-3, **8**
Krishnamoorthy, S.: AC-MoM-7, 2; AC-MoP-10, 4; DI-TuA-12, 7; DI-TuA-13, 7; EP-WeM-8, 9; MD-TuP-1, 8; TM-MoA-13, 3; TM-MoA-14, 3; TM-TuM-8, 6
Krishnan, G.: HM-MoP-4, 5
Kuball, M.: EP2-WeM-11, 9; TM-MoA-11, 3
Kuchuk, A.: DI-MoP-1, 4
Kuehne, P.: AC-MoM-8, 2
Kühne, P.: AC-MoP-4, 4
Kumagai, Y.: KEY1-2, 2
Kumar, A.: TM-MoA-14, 3
Kumar, S.: EP2-WeM-11, 9; KEY1-2, 2
Kuramata, A.: AC-TuM-15, 6; ET-MoP-3, 4
Kuznetsov, A.: MD-MoA-6, 3

— L —

Laccheb, M.: AC-MoP-7, 4
Lang, A.: MD-MoA-4, 3
Lang, A.: HM-MoP-2, 4

Langørgen, A.: TM-MoA-12, 3
Lawson, J.: EP-WeM-4, 9; MD-TuP-7, 8
Leach, J.: TM-TuM-8, 6
Lee, H.: EP-WeM-7, 9; ET-MoP-1, 4
Leedy, K.: DI-TuA-14, 7; DI-TuA-9, 7; EG-TuP-7, 8; EP-WeM-7, 9
Levin, A.: AC-MoM-7, 2
Li, J.: AC-MoP-1, **4**
Li, M.: TM-MoA-11, 3
Li, Q.: EP-MoP-2, 4
Li, W.: EP2-WeM-13, 9; MD-MoA-3, 3
Li, X.: MD-MoA-1, **3**
Liang, J.: KEY1-2, 2
Liao, M.: HM-MoP-1, **4**; MD-TuP-4, **8**; TM-MoA-13, 3
Liddy, K.: DI-TuA-14, 7
Liddy, K.: AC-MoP-11, 4; DI-TuA-9, 7; EP2-WeM-12, 9; EP-MoP-2, 4; EP-MoP-3, 4; EP-WeM-7, 9
Liu, D.: TM-MoA-11, 3
Lu, G.: DI-TuA-11, 7
Lubin, C.: AC-MoP-7, 4; TM-TuP-6, 8
Luccioni, D.: MD-TuP-4, 8
Lundh, J.: MD-TuP-3, 8
Lyons, J.: TM-TuM-7, 6; TM-TuP-4, **8**

— M —

Ma, Z.: HM-MoP-3, **4**
Macková, A.: MD-MoA-6, 3
Mahadik, N.: AC-TuM-15, **6**
Maimon, O.: EP-MoP-2, **4**
Manjeshwar, A.: TM-MoA-14, 3
Masten, H.: MD-TuP-3, **8**
Mastro, M.: ET-MoP-3, 4
Matto, L.: MD-TuP-4, 8
Mauze, A.: AC-MoP-9, 4; EG-TuA-3, 7
Mazumder, B.: AC-TuM-13, 6
McCandless, J.: AC-MoP-11, 4; EG-TuA-4, 7; EG-TuP-2, 8; EG-TuP-6, **8**; EP-MoP-4, 4
McCloy, J.: AC-MoP-10, 4; AC-MoP-6, 4; AC-MoP-8, 4; BG-MoM-12, 2
McCluskey, M.: AC-MoP-6, 4; AC-MoP-8, 4
McGlone, J.: AC-MoM-5, 2; EP2-WeM-10, 9
McGray, C.: TM-TuM-8, 6
Meng, L.: AC-TuM-13, 6; EP2-WeM-10, 9; MD-MoA-7, 3
Merrett, J.: MD-TuP-7, 8
Merrett, N.: EP-WeM-4, 9
Meyer, D.: EG-TuP-5, 8; HM-MoP-2, 4
Michaels, J.: MD-MoA-1, 3
Miesle, A.: DI-TuA-9, 7
Mikšová, R.: MD-MoA-6, 3
Mishra, A.: EP2-WeM-11, 9
Mishra, U.: MD-MoA-5, 3
Mock, A.: AC-MoP-9, 4
Mohammad, A.: EG-TuP-8, 8
Mondal, A.: EG-TuP-3, **8**
Morell, B.: EG-TuP-6, 8
Morgan, T.: DI-MoP-1, 4
Moser, N.: EP2-WeM-12, 9; EP-MoP-2, 4; EP-MoP-3, 4
Mou, S.: AC-MoP-1, 4; AC-MoP-12, 4; AC-MoP-7, 4; BG-MoM-14, 2; DI-TuA-9, 7; EG-TuA-4, 7; EP-WeM-7, 9

Moule, T.: EP2-WeM-11, 9
Mu, F.: HM-MoP-1, 4
Mu, S.: AC-MoM-8, 2
Muller, D.: MD-TuP-6, 8
Murakami, H.: KEY1-2, 2
Muralidharan, R.: EG-TuP-10, 8
Myers, R.: ET-MoP-2, 4; TM-TuP-2, 8

— N —

N Nath, D.: EG-TuP-10, 8
Nandi, A.: EG-TuP-3, 8
Nathaniel, J.: MD-MoA-4, 3
Neal, A.: AC-MoP-1, 4; BG-MoM-14, 2; DI-TuA-9, 7; EG-TuA-4, 7; EG-TuP-6, 8; TM-MoA-9, **3**
Nepal, N.: EG-TuP-5, **8**; HM-MoP-2, 4
Nguyen, P.: MD-MoA-6, 3
Nomoto, K.: EP2-WeM-13, 9; MD-MoA-3, 3
Noor, M.: MD-TuP-8, 8

— O —

O'Hayre, R.: EP-MoP-1, 4
Okay, A.: EG-TuP-8, 8
Orishchin, N.: DI-MoP-1, 4
Oshima, Y.: AC-MoP-9, 4
Osinsky, A.: BG-MoM-15, **2**
Osinsky, A.: DI-MoP-1, 4; DI-MoP-2, 4; EG-TuP-9, 8; EP-MoP-3, 4; HM-MoP-3, 4; MD-TuP-1, 8; MD-TuP-3, 8
Ou, X.: HM-MoP-1, 4

— P —

Pancotti, A.: AC-MoP-7, 4; TM-TuP-6, **8**
Park, A.: AC-TuM-14, 6
Pasayat, S.: DI-MoP-2, **4**; HM-MoP-3, 4
Pearton, S.: MD-MoA-4, 3
Peelaers, H.: TM-TuM-4, **6**
Peterson, C.: DI-TuA-12, 7; MD-TuP-1, **8**
Petkov, A.: TM-MoA-11, **3**
Pookpanratana, S.: EP-MoP-2, 4
Popp, A.: EP-WeM-5, 9; EP-WeM-7, 9
Porter, L.: AC-TuM-14, 6
Price, A.: EP2-WeM-10, 9
Protasenko, V.: AC-MoP-12, 4; EG-TuP-6, 8
Prytz, Ø.: MD-MoA-6, 3; TM-MoA-12, 3

— Q —

Qin, Y.: DI-TuA-11, 7

— R —

Raghavan, S.: EG-TuP-10, 8
Rajan, S.: DI-TuA-10, 7; EP2-WeM-10, 9; ET-MoP-2, 4; PS1-TuM-2, **6**; TM-TuP-2, 8
Rajapitamahuni, A.: TM-MoA-14, 3
Ramdin, D.: EP2-WeM-13, 9; MD-TuP-8, 8
Ranga, P.: AC-MoM-7, 2; AC-MoP-10, 4; EP-WeM-8, 9; TM-MoA-13, 3; TM-MoA-14, 3
Rehm, J.: EG-TuA-7, 7
Remple, C.: AC-MoP-6, **4**; AC-MoP-8, 4
Reunchan, P.: TM-TuM-6, 6
Richter, C.: EP-MoP-2, 4
Richter, S.: AC-MoM-8, 2; AC-MoP-4, **4**; AC-MoP-9, 4

Author Index

Rim, Y.: ET-MoP-1, 4
 Ringel, S.: AC-MoM-5, **2**; EP2-WeM-10, 9
 Rivera, J.: AC-MoP-3, 4
 Robinson, J.: HM-MoP-4, 5
 Roy, S.: DI-TuA-12, **7**; EP-WeM-8, 9; MD-TuP-1, 8
 Rudie, J.: DI-MoP-1, 4

— S —

S Chavan, P.: EG-TuP-10, 8
 Sabino, F.: TM-TuM-6, 6
 Saha, S.: MD-MoA-7, **3**
 Salamo, G.: DI-MoP-1, 4
 Sanders, M.: EP-MoP-1, 4
 Sandre Kilian, A.: TM-TuP-6, 8
 Sardar, A.: EP-WeM-4, **9**
 Sarker, J.: AC-TuM-13, **6**
 Sasaki, K.: AC-TuM-15, 6; DI-TuA-11, 7; ET-MoP-3, 4
 Scarpulla, M.: AC-MoM-7, **2**; AC-MoP-10, 4
 Schlom, D.: EG-TuA-4, 7; EG-TuP-2, 8
 Schubert, M.: AC-MoM-8, **2**; AC-MoP-2, 4; AC-MoP-3, 4; AC-MoP-4, 4; AC-MoP-9, 4; TM-TuP-3, 8
 Schwarzkopf, J.: EG-TuA-7, 7
 Scott, C.: BG-MoM-10, **2**
 Senckowski, A.: AC-MoM-5, 2; AC-TuM-12, 6
 Sensale-Rodriguez, B.: AC-MoP-10, 4
 Sepelak, N.: DI-TuA-9, 7; EP2-WeM-12, 9; EP-MoP-3, 4; EP-WeM-7, **9**
 Seyidov, P.: EG-TuA-7, 7
 Sharma, S.: AC-MoM-5, 2
 Shi, J.: HM-MoP-1, 4
 Shigekawa, N.: KEY1-2, 2
 Shin, M.: TM-TuP-6, 8
 Shoemaker, D.: TM-TuM-8, 6
 Singh, K.: EP-MoP-3, 4
 Singiseti, U.: AC-MoM-5, 2; MD-MoA-7, 3; TM-MoA-14, **3**; TM-TuP-1, 8
 Sinnott, S.: HM-MoP-4, 5
 Sleezer, R.: DI-MoP-1, 4
 Slocum, M.: AC-MoP-12, 4
 Smith, K.: MD-MoA-3, 3
 Smith, M.: EP2-WeM-11, 9
 Snyder, D.: AC-MoP-5, **4**; BG-MoM-13, **2**
 Soheli, S.: EP-MoP-1, 4
 Song, Y.: TM-TuM-8, 6

Soukiasian, P.: AC-MoP-7, 4; TM-TuP-6, 8
 Speck, J.: AC-MoP-9, 4; DI-TuA-13, 7; DI-TuA-14, 7; EG-TuA-1, 7; EG-TuA-3, 7; EG-TuP-9, 8
 Spencer, J.: DI-TuA-11, 7; ET-MoP-3, **4**; MD-TuP-3, 8
 Stanishev, V.: AC-MoM-8, 2
 Steele, J.: EG-TuP-2, **8**
 Steinbrunner, E.: BG-MoM-14, 2; EG-TuP-6, 8
 Stevens, K.: BG-MoM-10, 2
 Stokey, M.: AC-MoM-8, 2; AC-MoP-2, 4; AC-MoP-3, 4; AC-MoP-9, **4**; TM-TuP-3, 8
 Sturm, C.: ET-MoP-2, 4; TM-TuP-2, 8
 Subramanyam, G.: DI-TuA-9, 7
 Suga, T.: HM-MoP-1, 4
 Sutherland, D.: MD-TuP-6, 8

— T —

T. Sadowski, J.: TM-TuP-6, 8
 Tadjer, M.: MD-MoA-4, 3
 Tadjer, M.: AC-TuM-15, 6; DI-TuA-11, 7; ET-MoP-3, 4; MD-TuP-3, 8
 Taheri, M.: MD-MoA-4, 3
 Tanen, N.: EG-TuP-6, 8
 Tang, J.: AC-TuM-14, **6**
 Tetlak, S.: AC-MoP-11, 4; AC-MoP-12, 4; DI-TuA-9, 7; EP-MoP-4, 4
 Tetzner, K.: EP-WeM-5, **9**
 Thøgersen, A.: TM-MoA-12, 3
 Thompson, M.: AC-MoP-11, 4; AC-MoP-12, 4; EP-MoP-4, 4; EP-WeM-7, 9; MD-MoA-3, 3; MD-TuP-6, 8
 Thoutam, L.: TM-MoA-14, 3
 Tran Thi Thuy, V.: EG-TuA-7, 7
 Traouli, Y.: AC-MoP-3, 4
 Trdinich, Z.: HM-MoP-4, 5
 Tu, T.: ET-MoP-3, 4
 Turker, F.: HM-MoP-4, 5

— U —

Uren, M.: EP2-WeM-11, 9

— V —

Van de Walle, C.: AC-MoM-8, 2
 van Dover, R.: MD-TuP-6, 8
 Varley, J.: TM-TuM-7, 6
 Venkatachalapathy, V.: MD-MoA-6, 3
 Verma, D.: ET-MoP-2, **4**; TM-TuP-2, 8

Vincent, G.: HM-MoP-3, 4
 Vines, L.: MD-MoA-6, 3; MD-TuP-5, 8; TM-MoA-12, 3
 Vogt, P.: EG-TuA-4, 7
 von Wenckstern, H.: TM-MoA-12, 3

— W —

Walker, D.: EP2-WeM-12, 9
 Wang, B.: DI-TuA-11, **7**; TM-TuP-5, 8
 Wang, G.: DI-MoP-2, 4
 Wang, W.: DI-TuA-9, 7; EP-WeM-7, 9
 Wang, Y.: HM-MoP-1, 4; TM-MoA-13, 3
 Wang, Z.: KEY1-2, 2
 Ware, M.: DI-MoP-1, **4**
 Weber, M.: AC-MoP-8, 4
 Wells, J.: TM-MoA-12, 3
 Wetherington, M.: HM-MoP-4, 5
 Wheeler, V.: EG-TuP-5, 8; HM-MoP-2, **4**
 Whittier, C.: HM-MoP-4, 5
 Wickramaratne, D.: TM-TuM-7, **6**
 William, J.: EP-WeM-7, 9
 Williams, E.: AC-MoP-3, **4**
 Williams, J.: DI-TuA-14, 7; EP2-WeM-12, 9; EP-MoP-3, **4**
 Willis, B.: EG-TuP-8, 8
 Wong, M.: AC-MoM-5, 2; AC-MoP-1, 4; AC-TuM-12, 6
 Würfl, J.: EP-WeM-5, 9

— X —

Xiao, M.: DI-TuA-11, 7
 Xing, G.: EP2-WeM-13, 9; MD-MoA-3, 3
 Xing, H.: AC-MoP-9, 4; EG-TuA-4, 7; EG-TuP-2, 8; EG-TuP-6, 8; PS2-WeM-2, **9**
 Xu, W.: HM-MoP-1, 4

— Y —

Yadav, M.: EG-TuP-3, 8
 Yang, H.: AC-MoM-7, 2
 You, T.: HM-MoP-1, 4

— Z —

Zakutayev, A.: EP-MoP-1, 4
 Zamani-Alavijeh, M.: DI-MoP-1, 4
 Zhang, Y.: AC-MoP-9, 4; DI-TuA-11, 7; EG-TuA-3, 7; ET-MoP-3, 4; TM-TuP-5, 8
 Zhao, H.: AC-TuM-13, 6; EG-TuA-5, **7**; EP2-WeM-10, 9; MD-MoA-7, 3
 Zhu, W.: EP-WeM-7, 9